



Research Article

## Thermal and dynamic characterization of a multi-jet system with different geometry diffusers

Naas ZAHOUT<sup>1</sup>, Mohamed BRAIKIA<sup>1</sup>, Ali KHELIL<sup>1,\*</sup>, Hassane NAJI<sup>2</sup>

<sup>1</sup>University of Chlef, Laboratory of control, Testing, Measurement and Mechanical Simulation, 2000 Chlef, B. P. 151, Algeria

<sup>2</sup>Univ. Artois, Univ. Lille, IMT Lille-Douai, Junia, ULR 4515 - LGCg, Technoparc Futura, Béthune, F-62400, France

### ARTICLE INFO

#### Article history

Received: 17 March 2023

Revised: 22 April 2023

Accepted: 22 May 2023

#### Keywords:

CFD; Circular Jet; Experimental Study; Lobed Jet; SST k- $\omega$  Turbulence Model; Swirling Jet; Thermal Homogenization

### ABSTRACT

This paper proposed to use the impinging jets mixing process to improve the quality of residential heating and air conditioning. The main objective is to meet the requirements of occupants in terms of thermal comfort and air quality by proposing an optimal solution for the thermal homogenization improvement in the rooms by changing of the diffusers geometry and their arrangement in the ventilation and air-conditioning devices in blowing systems. This study involves both experimental and numerical studies of a three diffusers configurations composed of four peripheral jet with similar geometries and a central jet with a different geometry. All the configurations consist of four equidistant peripheral swirling jets, only the central jet that makes the difference between them. The configuration 1 includes a swirling central jet, on the other hand a circular central jet for the configuration 2 and finally a lobed central jet for configuration 3. The velocity and temperature distributions of the three configurations are investigated experimentally and numerically. Experimentally, the multifunction thermo-anemometer have been used to measure flow temperature and velocity. The dynamic and temperature features are more radially spread and get better homogeneity in configuration 3 and this is due to the energy distribution on the radial plane, which is relatively better than configuration 1 and configuration 2. The second part deals with numerical predictions of the dynamics and thermal fields of the three configurations considered. The study was realized using a RANS-based turbulence model. The numerical results are in reasonable agreement with our experiments for the three configurations. With this study, detailed information on the structure of the resulting flow is very useful to deepen the understanding of the physics of jet interaction and to validate turbulence models. The turbulence simulation is realized by the k- $\omega$ -SST model. This model gives a satisfactorily predicts the axial drop in velocity and temperature over the entire study range, demonstrating its ability to handle the interaction between swirling and lobe jets. Our results show that the geometry of the central diffuser is essential. This allows the axial velocity to decrease faster than configurations 1 and 2. This increases lateral diffusion, resulting in better homogenization.

**Cite this article as:** Zahout N, Braikia M, Khelil A, Naji H. Thermal and dynamic characterization of a multi-jet system with different geometry diffusers. J Ther Eng 2024;10(2):404–429.

#### \*Corresponding author.

\*E-mail address: a.khelil@univ-chlef.dz

This paper was recommended for publication in revised form by Editor-in-Chief Ahmet Selim Dalkılıç



## INTRODUCTION

The mixing process depends on the turbulence intensity. These turbulent jets have a great importance in scientific research because of their use in a wide variety of industrial processes. The stated process include a jet engine thrust, pollutant dispersion, drying paper, textiles, ceramics, cooling electronic components, ventilation and heating and air conditioning systems used in the premises. The most of recent studies have been done on turbulent jets using certain methods such as theoretical, numerical and experimental. Of the three methods, the computational fluids mechanics system is fairly cheaper, brisk and light. The computational fluids mechanics are used in numerical simulation for the engineering problems using a set of equations which are called governing equations. Recent developments in the performance of computers have made a bigger revolution in computational methods. One of the similar computational systems that grew fleetly is Computational Fluid Dynamics (CFD). Due to the efficient operation and familiarity of this system among experimenters, there have been many developments in the field of numerical methods applied to fluid mechanics. [1,2].

The main objective of ventilation systems is to meet the requirements of occupants in terms of thermal comfort and air quality. However, this must be achieved by using as little energy as possible. The three design requirements must be taken into account, as they are crucial for the thermal environment and energy efficiency. A high level of induction is essential for mixing ventilation as it ensures optimal mixing of the ventilation jet with ambient air, ensuring that occupants are satisfied in terms of thermal comfort and air quality. During the past few decades, it has become apparent that the generation of vortices in a mixing flow using certain vortex generators such as lobe and/or swirl nozzles is an extremely strong mechanism for enhancing flow mixing. To ameliorate the diffusion efficiency at a lower cost taking into account the aesthetic aspect of the devices designed, a passive system blowing the jet through the lobed or the swirling diffuser is a good alternative. Their applications are very wide. These include jet engine thrust, pollutant dispersion, air conditioning, ventilation and heating systems used in the building. Impinging jets are used in several applications, such as air conditioning, cooling of food products, drying of textiles and paper and cooling of electronic equipment. The impinging jets provide suitable flow from specially designed nozzles while ensuring suitable mixing. In addition, the mixing process is often related to the turbulence intensity involved. A recent study concluded that the homogenization process using swirling or lobed diffusers is an extremely powerful mechanism for enhancing flow mixing. These lobed diffusers generally consist of a splitter plate with a wavy trailing edge. The air diffusers are used in order to enhancing the mixing of the flows in the atmospheres. This operation provides clean air and

maintains comfortable thermal conditions for building occupants in terms of air quality, thermal comfort and energy consumption.

Therefore, innovative diffusers must be designed to enhance mixing. In passive hybrid ventilation control, multi-leaf vents in ceiling diffusers with perforated panels have been shown to produce more pronounced induction. This suggests that the passive system blowing lobed jets may be a good technique to improve the flow diffusion efficiency. It should be noted that enhancing mixing through passive control has important practical implications for jet engines, pollutant transport, paper drying, textiles, ceramics, electronics, refrigeration, air conditioning, ventilation and heating of buildings [3- 5]. The main purpose is to understand the physics of the interaction of jets blown through diffusers with different geometries. This study highlights effective ways to enhance the self-induction jets for their integration in the terminal units of the cooling, cooling and heating devices. With this in mind, much research has been carried out to improve the efficiency of the diffusion of dynamic and thermal fields using active and passive techniques for turbulent jets. In the first step, the importance and the role of the diffuser geometry of the central jet relative to the peripheral jets in the thermal and dynamic field of the resulting lobed jet has been shown. In the second step, a three dimensional numerical simulation study of several configurations of multiple jets made up of five diffuser jets have been developed. The compatibility of turbulence models with this type of flow has been tested. The document is divided into five parts. The first part consists of a bibliographical study and the second part is devoted to the experimental part by describing the experimental installation carried out with the different blowing devices studied. The third part is intended for the numerical simulation of the different configurations studied, on the other hand the fourth part was intended for the discussion of the results. Ends with a general conclusion summarizing the main results of this work. Jets are one of the most studied flows due to their many industrial applications. Several experimental and numerical studies were investigation with the purpose of a better understanding of the physical phenomena concerned.

Kravtsov et al. [6] experimentally investigated the flow structure and mixing in the initial region of a swirling turbulent jet using the particle image velocimetry and planar laser-induced fluorescence techniques for velocity and concentration measurements. Three cases of swirling rate were considered, namely jet without swirling, low swirling jet without central recirculation zone and high swirling jet. The vortex has been observed to result in a wider spray and improved mixing. Turbulent jet issued from a lobed diffuser have been experimentally investigated by Meslem and Nastase [7]. They compared their findings to those of an axisymmetric jet with the same initial volumetric flow and exit area. They concluded that the entrainment rate is

due to the asymmetric shape of the nozzle and the strong convection of the turbulent structures induced by the lobes. Medaouar et al. [8] performed a combined experimental and computational study of a central lobed jet surrounded by six equidistant peripheral lobed jets, and found that the interaction between the jets leads to velocity and temperature redistribution in the mixed zone, while allowing the propagation of the resulting jet. Feli et al. [9] experimentally studied the dynamics of impinging turbulent jets produced by inclined blades. They observed that the blade wall changed the shape of the swirling jet, causing it to spread outward and create a recirculation zone around the blade seat, where the vortex takes place before the blade surface collapses.

Lee [10] compared the swirl angle disintegration characteristics of internal mixing pneumatic nozzles under different operating conditions. Therefore, four internal swirl mixing nozzles with axisymmetric holes at swirl angles of 15°, 30°, 45° and 60° to the central axis are used to enhance the mixing of the aerodynamic jet. This shows that the atomization characteristics work well at the vortex angle of 30°, and the turbulence intensity gradually decreases with the increase of the azimuth spacing. In particular, it has been shown that the nozzle configuration is an important geometric parameter affecting the jet trajectory.

Meslem et al. [11] presented an innovative concept of optimized air distribution to improve mixed ventilation in buildings. The method used is to passively control the air jet through a lobe diffuser. All of their results lead to the same result. Lobe diffusers favor self-induction compared to conventional circular perforated diffusers.

Meslem et al. [12] concluded that when using jets in the mixing process, large entrainment is required, especially near the jet exit. According to the authors, many studies have shown the superiority of the mixing performance of non-circular nozzles. It is noted that complex jet-mixing layer operations are achieved by lobe nozzles and that lobe-jet mixing flows have been extensively previously studied over the past 30 years at high Reynolds numbers for combustion and aeronautical applications. According to some authors, such geometries are attractive to the heating, ventilation, and air conditioning (HVAC) field because of their relative aesthetics, low cost, and hybrid efficiency.

Bennia et al. [13] also carried out a comparative study of the performance of different diffuser geometries. By evaluating the axial velocity profiles of the jet and the comparison of the lobed jet using different lobe geometries shows that a diffuser with inclined lobes homogenizes the airflow relatively ameliorate in the experimental room than a lobed diffuser with a cross-section. Nuntadusit et al. [14] examined the local structure of turbulent swirling impinging jets experimentally. They founded that over the range investigated, the maximum Nusselt number is localized with multiple

swirling impinging jets at the jet-to-jet distance  $S/D=4$ . Stephane Maurel et al. [15] concluded that the development of a general correlation could predict the evolution of the axial velocity whatever the thickness of the jet and the distance to the impact. The results are compared and validated with experimental measurements obtained by laser Doppler anemometry. According to the distance  $H$  from the impact wall and the initial thickness of the jet, the development will be relatively differently because of confinement that determines the expansion of the jet. A stereo PIV (Particle image velocimetry) technique using advanced pre- and post-processing algorithms is implemented for the experimental study of the local structure of turbulent swirling impinging jets were used by Alekseenko and al. [16]. They investigated the influence of the PIV (Particle image velocimetry) finite spatial resolution on the measured dissipation rate, velocity moments and analyzed and compared with numerical predictions. For this purpose, they realized a special series of 2D PIV (Particle image velocimetry) measurements was carried out with vector spacing up to several Kolmogorov length scales. It was found that the magnitude of pressure diffusion decreased with the growth of the swirl rate. In general, the studied swirling impinging jets had a greater spread rate and a more rapid decay in absolute velocity when compared to the non-swirling jet. Xu et al. [17] used the LES method of swirling and non-swirling impinging jet from an orifice with four spiral and straight grooves. The local wall-adaptive turbulent viscosity model (WALEM) was chosen to study the relationship between the structure and the heat transfer properties of the square orifice and the spiral orifice for impinging jet cooling. They found that, compared to the 0° straight orifice, the 45° spiral orifice has a greater fluctuation velocity due to velocity deviation, resulting in greater turbulence intensity and greater airlift capacity. The intensity of the 45° spiral orifice heat transfer to the target surface is slightly expand between 5 and 10%. Kannan et al. [18] performed a numerical prediction of a turbulent free jet blown from an axisymmetric orifice in a static air environment. The numerical results determined by the standard  $k-\epsilon$  turbulence closure model are compared with the experimental measurements. They found that the advection increases to counteract dissipation, resulting in overestimation. The experimental approach uses time resolved and classical large scale PIV measurements have been used by Nastase et al. [19]. They showed that the jet flows from innovative rectangular air diffusion grilles with lobed ailerons ensure higher mixing in a room than baseline jets from classical rectangular air diffusion grilles with straight ailerons. Braikia et al. [20] carried out a study in which they examined various multiple swirling jet configurations. They stressed the significance of choosing an adequate air-diffuser location to increase the thermal homogeneity of the handled region. The center jet appears to have an important

function in improving thermal homogeneity. To summarize, the writers came to the following conclusion: The quality of ambient homogeneity is affected by the space between the jets and their sensation of rotation relative to the center jet, according to the findings of their investigation. The one with a swirling center jet directing the behavior of six swirling jets in counter-rotation is proven to be the most successful in terms of thermal de-stratification among the different configurations studied.

Khelil et al. [21] used the  $k-\epsilon$ , RNG  $k-\epsilon$  and RSM turbulence models to statistically investigate the interaction between numerous swirling jets deployed in uneven positions. They found that the RSM model was more suitable than the regular  $k-\epsilon$  model for capturing mean flow behavior after conducting a numerical examination. They demonstrated that the mixing between the swirling jets caused a temperature distribution along the centerline and near the blower diffusers while allowing the resulting jet to spread further. Bragança et al. [22] investigated thermal comfort and noise generation in a full-scale model room with mixing ventilation, heating mode, and cooling mode. A seated basic shape heated manikin in the center of the room has been used to imitate an inhabitant. A multi-cone diffuser (CD) flush-mounted in the center of the ceiling generates the ventilation jet in vertical and radial modes, respectively. The impact of inserted lobes in a diffuser that is LD has been studied. Thermal comfort is significantly improved in the presence of lobed inserts in the diffuser, whether in cooling or heating modes, according to an analysis based on both ASHRAE 55 and ISO 7730 standards. This was accomplished with little to no increase in pressure drop or noise. In addition to the performance provided by the concept of lobed inserts, it is simple to incorporate into the production process when compared to the built-in lobed diffuser. For these reasons, the concept of inserted lobes offers a viable low-cost approach for improving HVAC system performance. Mohan et al. [23] used the  $k-\epsilon$  turbulence model to execute a numerical investigation of many lobed jets. The increase process of the mixture by the multiple lobed jets was presented in this study. For the same quantity of momentum flux given at the nozzle intake, more research was done to compare the mixing enhancement of multiple lobed jets with that of multiple conventional round jets. The numerical predictions matched the experimental results fairly well. In the case of several lobed jets, the centerline velocity decay rate was the fastest. The strongest stream-wise vortices were created when several lobed jets were used. To determine the jet shape that delivers the best mixing, a passive scalar (temperature) was employed to quantify mixing. Multiple lobed jets performed the greatest mixing in the near field of the jet by introducing powerful streamwise vortices early; however, both jet topologies behaved similarly in the distant field of the jet. Bennia et al. [24] In order to examine the qualities of a lobed

diffuser in terms of homogenizing the atmosphere, the dynamic profiles on the main plane were compared with those on the secondary plane. Because of the lobes' larger opening, the scientists discovered that dynamics profiles in the potential core region are more distributed at the main plane. However, the dynamic profiles further from the central core are similar to those of a circular jet, demonstrating that the lobe shape had no effect. Boussoufi et al. [25] used the notion of entropy generation to examine the flow and interaction of numerous jets numerically. A single jet encircled by equidistant 3, 5, and 9 circumferential jets has been examined in several configurations. The major findings show that the CFD model is capable of accurately predicting flow patterns in many jets. The correlation between CFD forecasts and experimental outcomes is excellent.

The main goal of this investigation is to study the distribution of velocities and temperatures, first experimentally and then numerically, for three jet configurations. The first configuration is the central swirling jet surrounded by four equidistant peripheral swirling jets. The second configuration is the central circular jet surrounded by four peripheral swirling jets and the third configuration is the central lobe jet surrounded by four peripheral swirling jets. This type of flow has been studied with a view to developing new air diffusers for heating ventilating air conditioning systems for the purpose of providing comfort in residences and transportation.

The originality of this study is to meet the requirements of occupants in terms of thermal comfort and air quality by proposing an optimal solution for the thermal homogenization improvement field in the rooms by changing of the diffusers geometry and their arrangement in the ventilation and air-conditioning devices in blowing systems.

## EXPERIMENTAL SETUP

The experiments were carried out in a chamber of  $3.8 \times 3.5 \times 2.9 \text{ m}^3$  (LxWxH). The experimental installation is composed of a metal framework on which is fixed a Plexiglas plate. At the ceiling of the room, five devices with diffusers of different geometries blowing hot air are placed and directed downwards (Figure 1). The temperatures ( $T_i$ ) and the velocities ( $U_i$ ) of the jet are measured by a multifunctional thermo-anemometer (Velocicalc Plus type). The hot wire anemometer (type Velocicalc Plus Air velocity Meter) is a high-precision multifunctional instrument. The data can be viewed on a screen, printed or downloaded to a spreadsheet program allowing us to easily transfer data to a computer for statistical treatment. The accuracy is of order  $\pm 0.015 \text{ m/s}$  for velocity and for  $\pm 0.3 \text{ C}^\circ$  temperature from thermal sensor. The thermal sensor is supported by rods that are easily guided vertically and horizontally to scan a maximum space in all three directions. In addition, a digital

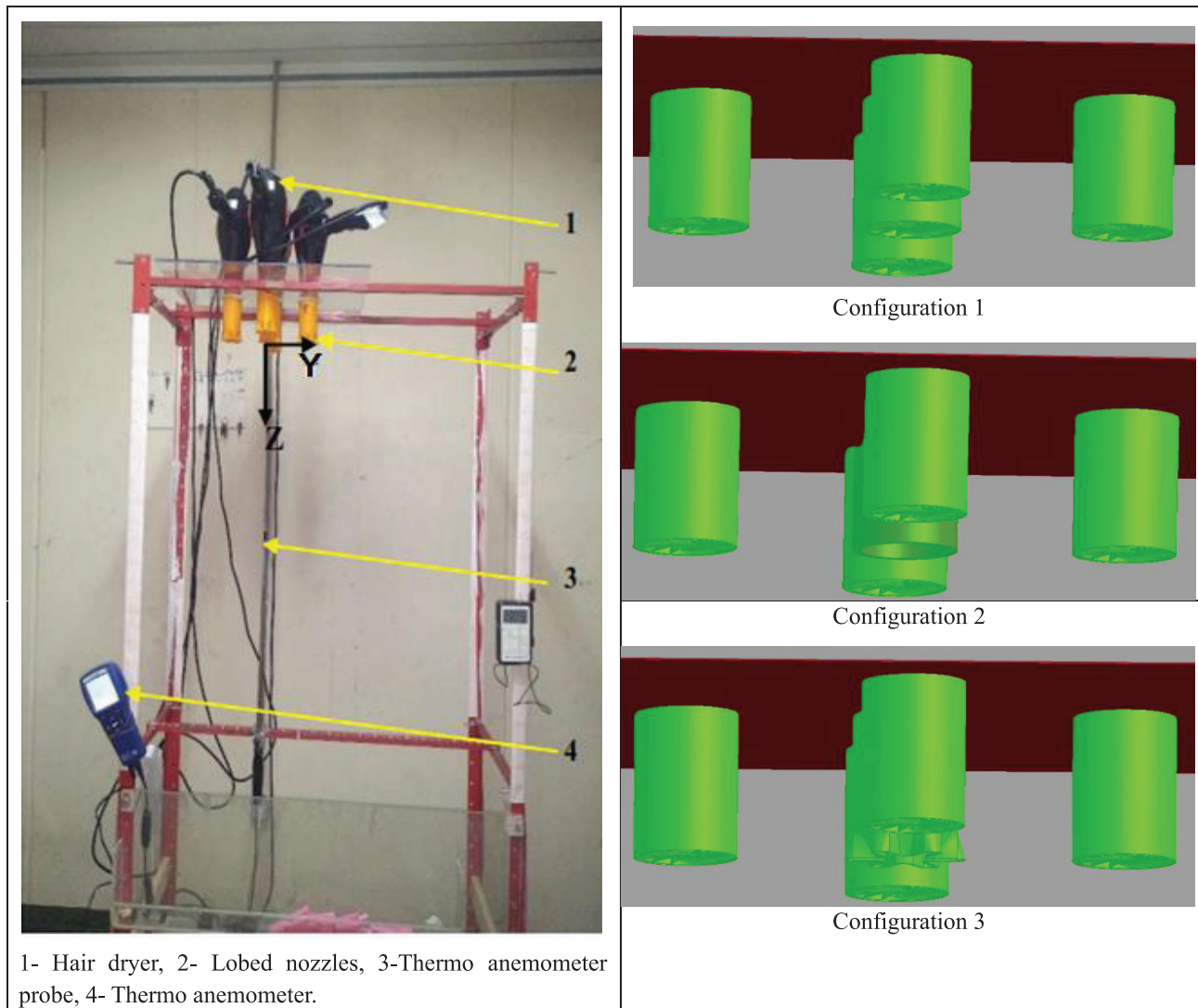


**Figure 1.** Experimental setup.

thermometer was placed (outside the jet) to instantly measure ambient temperature ( $T_a$ ).

Figure 2 displays the geometry of the swirl diffuser with twelve vanes disposed in a carrier with a diameter  $d$  of 0.022 m. To realize a swirl effect, the vanes are positioned at inclination angles of  $30^\circ$  and  $60^\circ$  with consideration to the jet axis and blowing plane, respectively. The vanes are disposed in such a way that they are connected to a fixed support (vane support) behind which a recirculation zone develops, the length of which depends on the blower having a diameter  $D$ , which is related to the diameter of the blowing origin.

Figure 3 shows the circular diffuser geometry used by 0.040m diameter.

Figure 4 shows the lobed diffuser geometry utilized in this work. The diffuser consists of a round tube with a length of 0.09 m and a diameter of 0.04 m and with a daisy-shaped

outlet. The blowing plane has six parallel-sided inclined lobes and six sinusoidal channels with  $22^\circ$  and  $14^\circ$  are the inner and outer penetration angles, respectively. The height of each is 0.015m and its width is 0.006m.

Figure 5 represents the three different configurations studied,  $Y/D=2.5$  is the spacing ratio between nozzles. The reference velocity  $U_0$  and temperature  $T_0$  measured at the jets' outflow are respectively 10 m/s and 325 K. The jet Reynolds number is  $2.5 \times 10^4$ .

### Computational Method and Meshing

#### Governing equations

Solving fluid dynamics equations in turbulent conditions considers averaging equations, mass conservation and quantity of motion conservation and energy conservation [26 and 27].

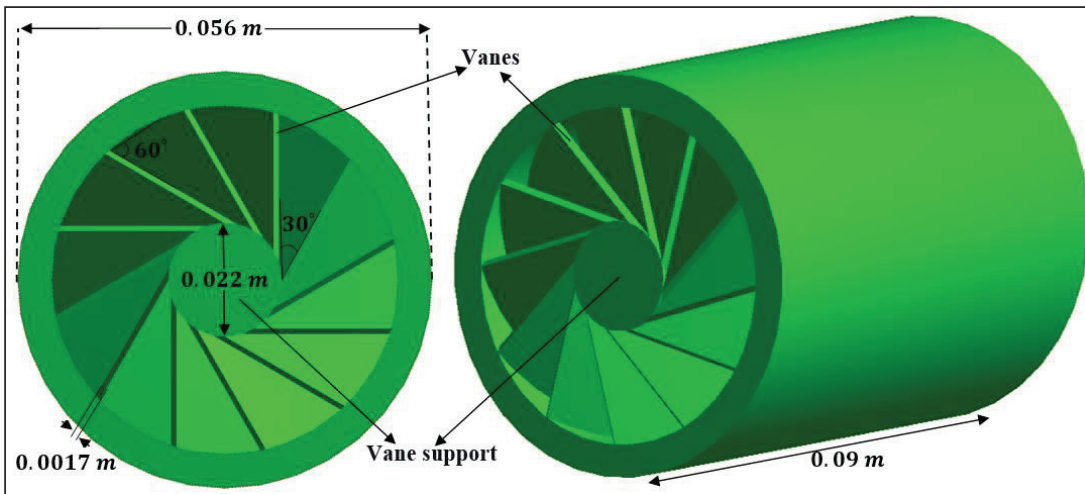


Figure 2. Sketch of swirling diffuser.

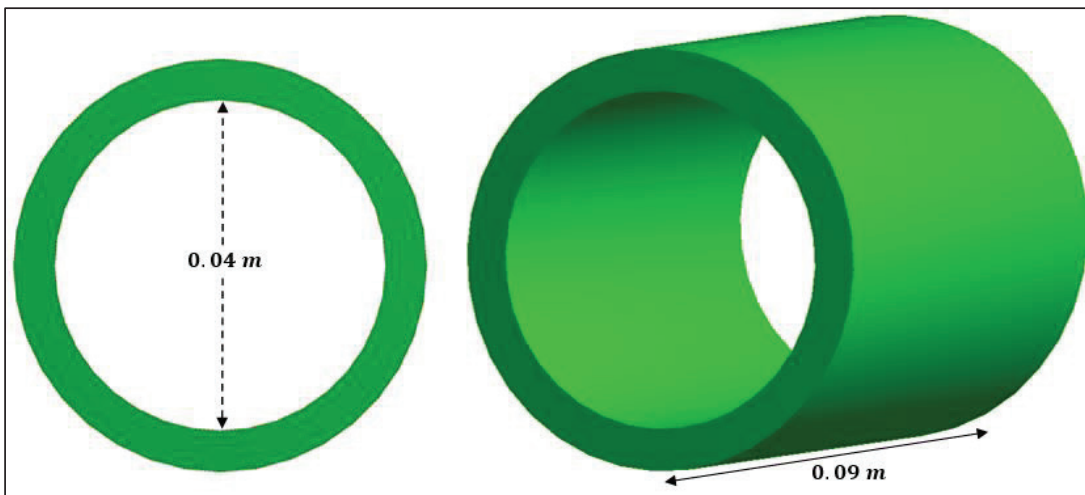


Figure 3. The circular nozzle.

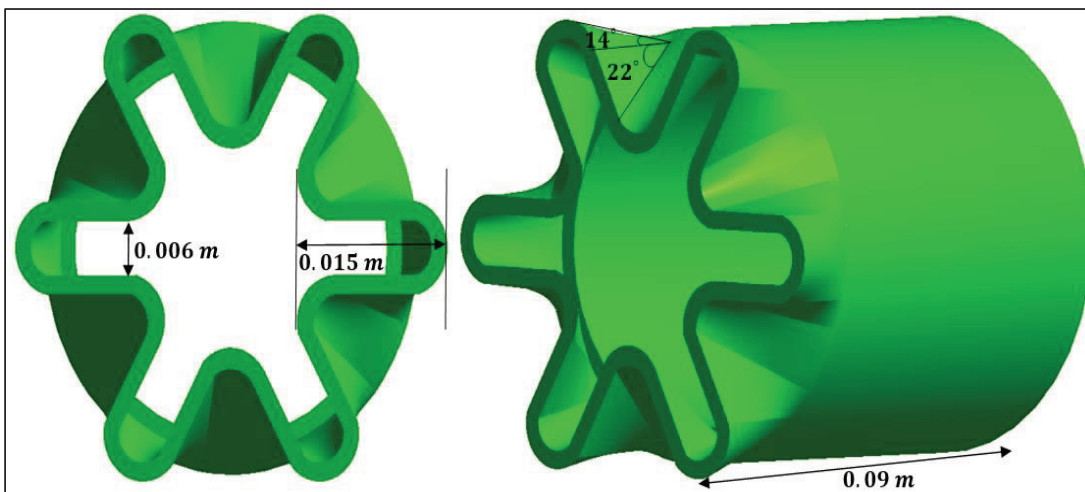
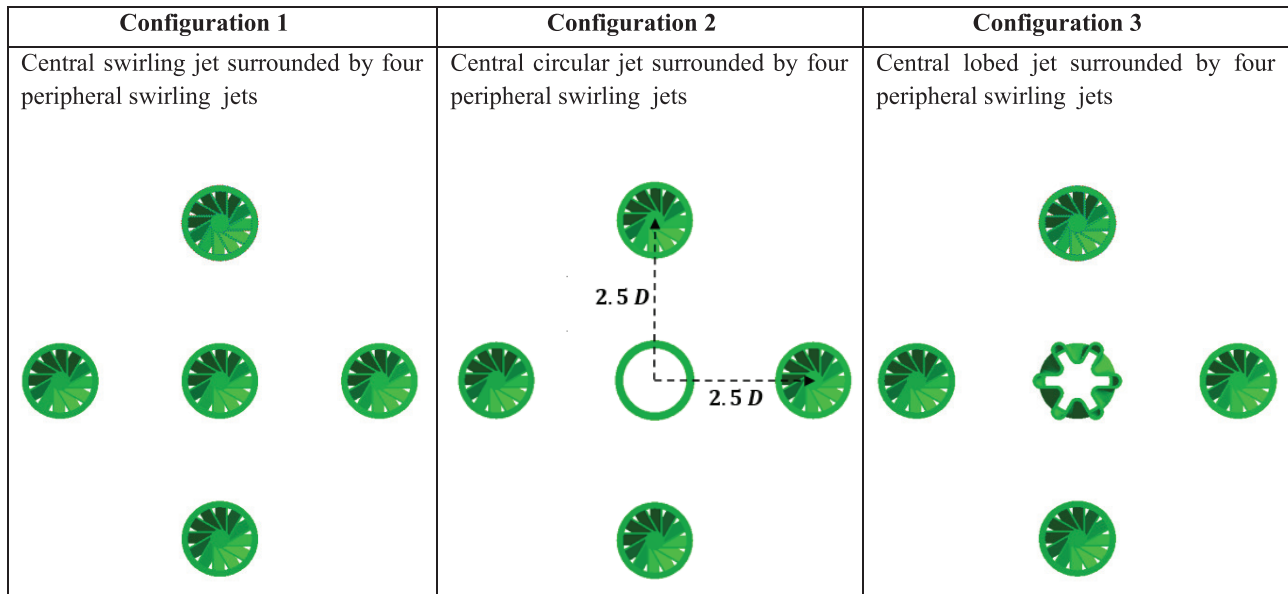


Figure 4. The lobed diffuser.



**Figure 5.** Schematic of the diffusers disposition for configuration 1, 2 and 3.

The equation of mass conservation is written as follows:

$$\frac{\partial \rho u_i}{\partial x_i} = 0 \quad (1)$$

The average momentum equation is written as follows:

$$\frac{\partial}{\partial x_j} (\rho u_j u_i) = -\frac{\partial P}{\partial x_i} + \frac{\partial}{\partial x_i} \left[ \mu \left( \frac{\partial u_i}{\partial x_j} + \frac{\partial u_j}{\partial x_i} \right) - \overline{\rho u_i' u_j'} \right] \quad (2)$$

The energy equation is written as follows:

$$\rho C_p u_i \frac{\partial T}{\partial x_i} = \frac{\partial}{\partial x_i} \left[ \lambda \frac{\partial T}{\partial x_i} - \rho C_p u_i' T' \right] \quad (3)$$

Mean velocity and temperature are represented by  $U_i$  and  $T$ , respectively, while other parameters include  $\mu$  for dynamic viscosity,  $\rho$  for fluid density,  $P$  for pressure,  $C_p$  for specific heat capacity at constant pressure,  $\lambda$  for thermal conductivity,  $u_i'$ ,  $u_j'$  and  $T'$  for corresponding fluctuation components,  $-\overline{\rho u_i' u_j'}$  and  $-\overline{\rho C_p u_i' T'}$  for average Reynolds stresses and turbulent heat fluxes. To obtain a complete set of equations, models for  $-\overline{\rho u_i' u_j'}$  and  $-\overline{\rho C_p u_i' T'}$  are required to close the equations.

## Mathematical models

### SST model K- $\Omega$

The shear stress transport (SST) model was proposed by Menter [28-30]. The transport equations for turbulence are written as follows:

a -Kinetic turbulence energy of k:

$$\frac{\partial k}{\partial t} + U_j \frac{\partial k}{\partial x_j} = \frac{\partial}{\partial x_j} \left[ \left( \nu + \sigma_k \nu_T \right) \frac{\partial k}{\partial x_j} \right] + P_k - \beta^* k \omega \quad (4)$$

b -Specific dissipation rate of  $\omega$ :

$$\begin{aligned} \frac{\partial \omega}{\partial t} + U_j \frac{\partial \omega}{\partial x_j} = & \alpha S^2 - \beta \omega^2 + \frac{\partial}{\partial x_j} \left[ \left( \nu + \sigma_\omega \nu_T \right) \frac{\partial \omega}{\partial x_j} \right] \\ & + 2(1 - F_1) \sigma_{\omega 2} \frac{1}{\omega} \frac{\partial k}{\partial x_i} \frac{\partial \omega}{\partial x_i} \end{aligned} \quad (5)$$

The viscosity of the kinematic tourbillon is given by:

$$\nu_T = \frac{\alpha_1 k}{\max(\alpha_1 \omega, SF_2)} \quad (6)$$

$F_1$  (Mixing function)

$$F_1 = \tanh \left[ \left[ \min \left[ \max \left( \frac{\sqrt{k}}{\beta^* \omega y}, \frac{500 \nu}{y^2 \omega} \right), \frac{4 \sigma_{\omega 2} k}{CD_{k\omega} y^2} \right] \right]^4 \right] \quad (7)$$

Note:  $F_1 = 1$  inside the boundary layer and 0 in the free flow.

$F_2$  (Second mixing function)

$$F_2 = \tanh \left[ \left[ \max \left( \frac{2\sqrt{k}}{\beta^* \omega y}, \frac{500 \nu}{y^2 \omega} \right) \right]^2 \right] \quad (8)$$

$P_k$  (Production limiter)

$$P_k = \min \left( \tau_{ij} \frac{\partial U_i}{\partial x_j}, 10\beta^* k\omega \right) \tag{9}$$

$$CD_{k\omega} = \max \left( 2\rho\sigma_{\omega 2} \frac{1}{\omega} \frac{\partial k}{\partial x_i} \frac{\partial \omega}{\partial x_i}, 10^{-10} \right) \tag{10}$$

$$\phi = \phi_1 F_1 + \phi_2 (1 - F_1) \tag{11}$$

**Solution Procedure**

The CFD code used for turbulence simulation is ANSYS it offers several options including flow simulation. Fluent

solves the three-dimensional Navier-Stokes equation, pressure, temperature, and turbulence using the controlled volume approach [31-35]. It was decided to use the implicit pressure-based solver. For pressure-velocity coupling, the SIMPLE algorithm is utilized.

**Boundary Conditions**

The boundary conditions of the turbulence models in this study were as follows:

- Entry velocity: 10 (m/s)
- Inlet temperature (K) 325.
- Intensity of turbulence: 5 (%).
- Reynolds Number: 25000
- Convergence criterion a: Energy =  $10^{-6}$ , other parameters =  $10^{-4}$ .

**Table 1.** SST k- $\omega$  model Constants

| $\sigma_{\omega 2}$ | $\sigma_{\omega 1}$ | $\sigma_{k 1}$ | $\alpha_1$ | $\beta_1$ | $\beta_2$ | $\alpha_2$ | $\beta^*$ | $\sigma_{k 2}$ |
|---------------------|---------------------|----------------|------------|-----------|-----------|------------|-----------|----------------|
| 0.856               | <b>0.5</b>          | 0.85           | 0.55       | 0.075     | 0.0852    | 0.44       | 0.09      | 1              |

**Mesh Generation**

Meshes can be drawn to be hexahedral or tetrahedral in general, depending on the domain complexity. Due to the geometric complexity of the nozzles, a tetrahedral mesh have been used in this case (Figure 6). It is important to

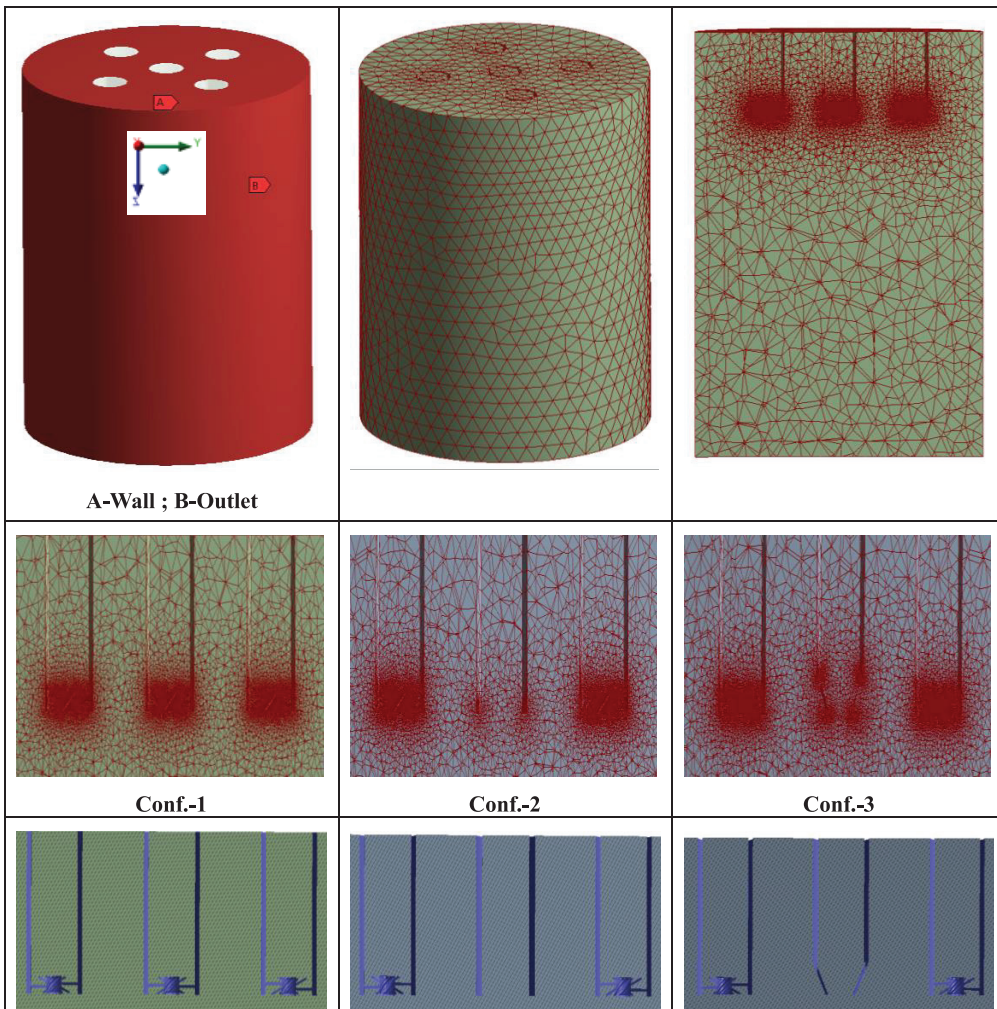


**Figure 6.** Computational domain meshing.

note that developing an organized grid can be challenging and time-consuming. As a result, the usage of unstructured grids is an option that, while requiring more memory, is acceptable for mapping complicated domains such as the one considered here.

**Mesh Independency**

Mesh quality and resolution play an important role in order to obtain a precise numerical solution and stability evaluated by the analysis of four different mesh sizes, the four mesh sizes are compared to experimental work. The

**Table 2.** Tested meshes

|        | Configuration 1 | Configuration 2 | Configuration 3 |
|--------|-----------------|-----------------|-----------------|
| Mesh 1 | 1070419         | 1105508         | 1080561         |
| Mesh 2 | 2164599         | 2039586         | 2018596         |
| Mesh 3 | <b>3156999</b>  | <b>3140909</b>  | <b>3264760</b>  |
| Mesh 4 | 4009138         | 4168878         | 4057547         |

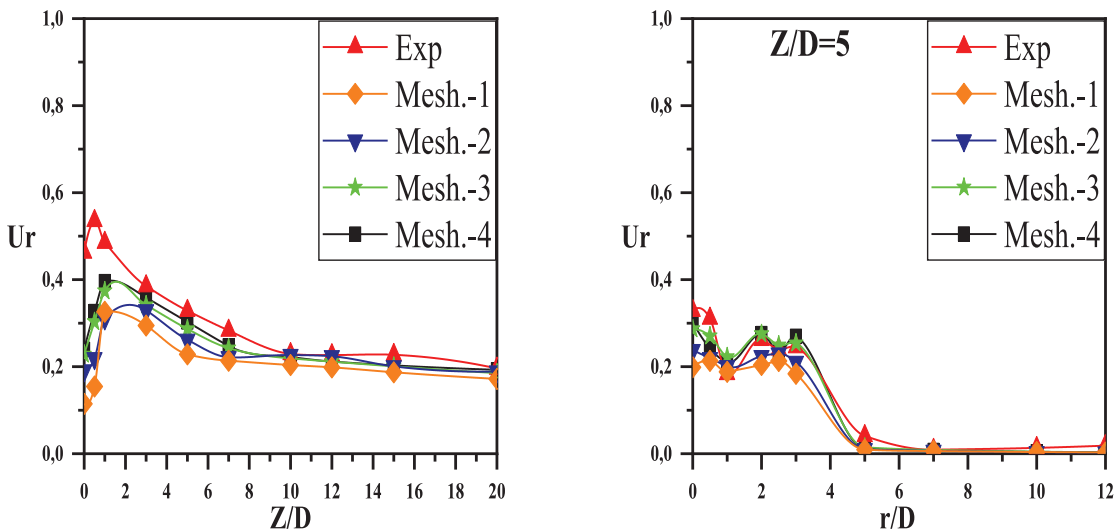


**Figure 7.** Mesh solution independence for axial and radial velocity obtained from the SST k- $\omega$  model (Configuration 1).

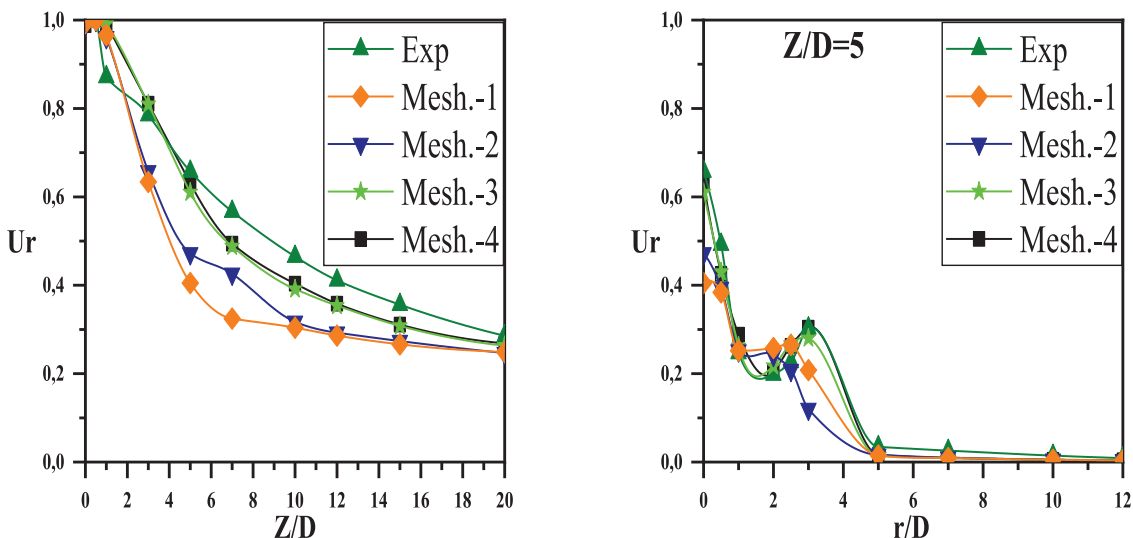


**Figure 8.** Mesh solution independence for axial and radial velocity obtained from the SST k- $\omega$  model (Configuration 2).

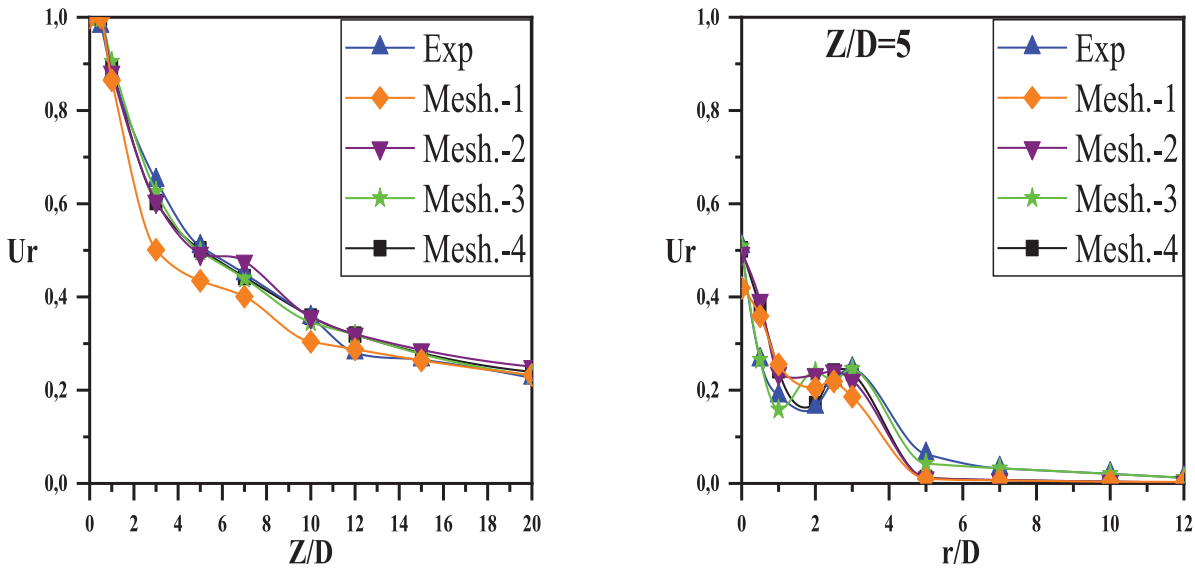


Figure 9. Mesh solution independence for axial and radial velocity obtained from the SST k- $\omega$  model (Configuration 3).

radial and axial velocity profiles simulated with mesh 3 accurately reflect the experimental data, as shown in Figure 7 to 9. As a result, mesh 3 is chosen to run the simulations.

**EXPERIMENTAL RESULTS AND DISCUSSIONS**

Figure 10 shows the velocity and temperature profiles at the axial level of the three configurations. Note that all three nozzles have the same equivalent diameter and operating conditions. Over an axial distance of 20 jet diameters from the nozzles outlet, velocity  $Ur = \frac{U_i}{U_0}$  and temperature

$Tr = \frac{T_i - T_a}{T_{in} - T_a}$  The induction produced by each jet causes a rapid drop in temperature and axial velocity, which stabilizes away from the blow sites for the three jets. Changes in velocity and temperature can be divided into three regions:  
 $Z / D < 1$  Velocity and temperature remain the same at initial and maximum because it is close to the blowing site.  
 $1 \leq Z / D \leq 7$  The velocity and temperature profiles decrease very quickly and this rapid decrease of the axial velocity explains the transfer of energy to the radial direction.

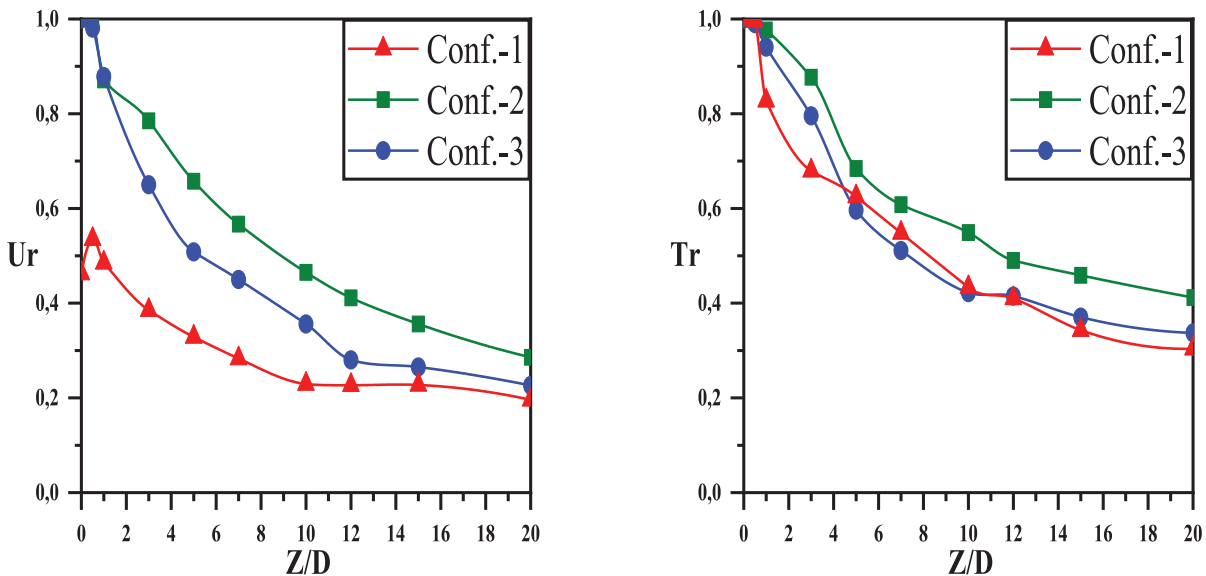


Figure 10. Axial profiles temperature and velocity for three configurations.

$7 < Z / D$  Changes in velocity and temperature profiles become small and somewhat regular.

Figure 11 shows the measured radial velocity profiles and Figure 12 shows the radial temperature profiles.

$r / D \leq 3$  In this region, the changes are very important because there are maximum values close to the nozzle outlet

outlet and minimum values far from the nozzle outlet. This indicates that the jets did not interact with each other.

$3 < r / D \leq 7$  The jets begin to interact with each other gradually, allowing a decrease in maximum values and an increase in minimum values.

$7 < r / D$  The radial velocity and temperature profiles begin to stabilize to show curves from a single jet.

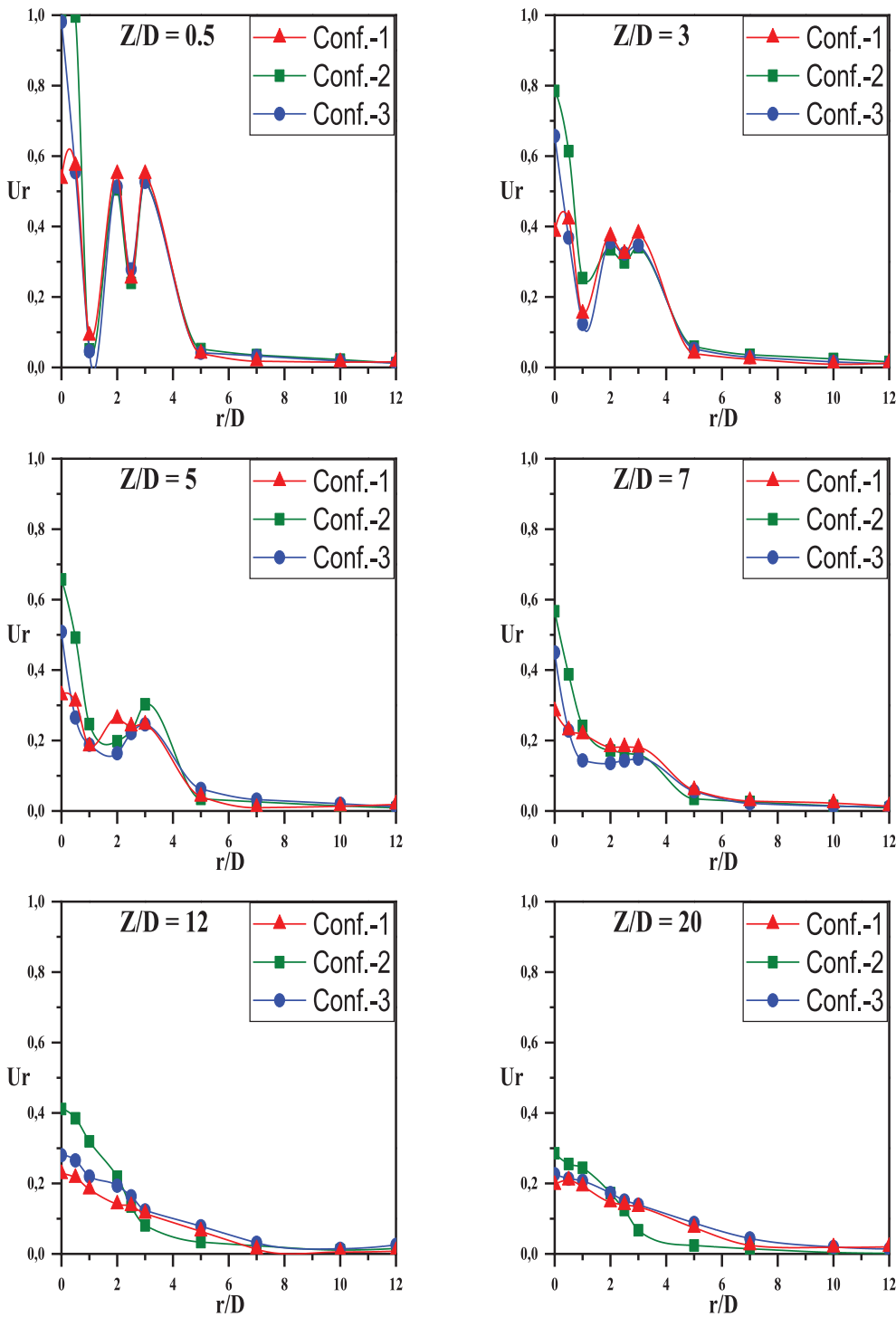


Figure 11. Radial velocity profiles for (three configurations).

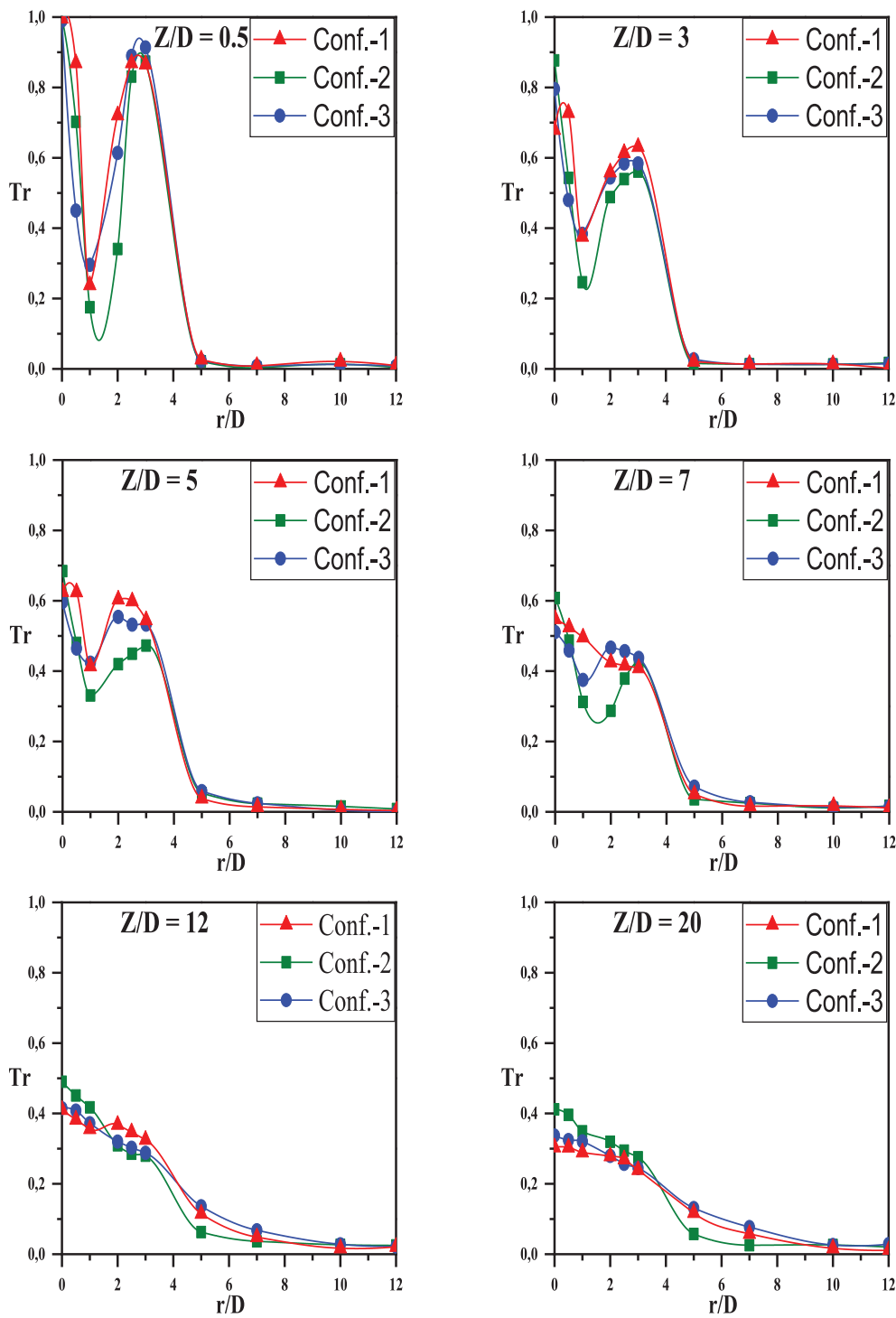


Figure 12. Radial temperature profiles for (three configurations).

### COMPUTATIONAL RESULTS AND DISCUSSIONS

Figure 13 provides a comparison between experimental and numerical results related reduced axial velocity ( $U_r$ ) and reduced temperature ( $Tr$ ) at different stations. The numerical results are obtained by the previous perturbation model. After station  $Z / D = 5$ , model SST k- $\omega$  Gives

a similar shape that shows more closeness with empirical values. The root mean square error (RMSE) between the results obtained with the model and the experimental results for the velocity profiles was 0.10226134, and the temperature was 0.06094824.

The results of the numerical simulation presented in Figs. 14 and 15 relate, respectively, to the evolution of the

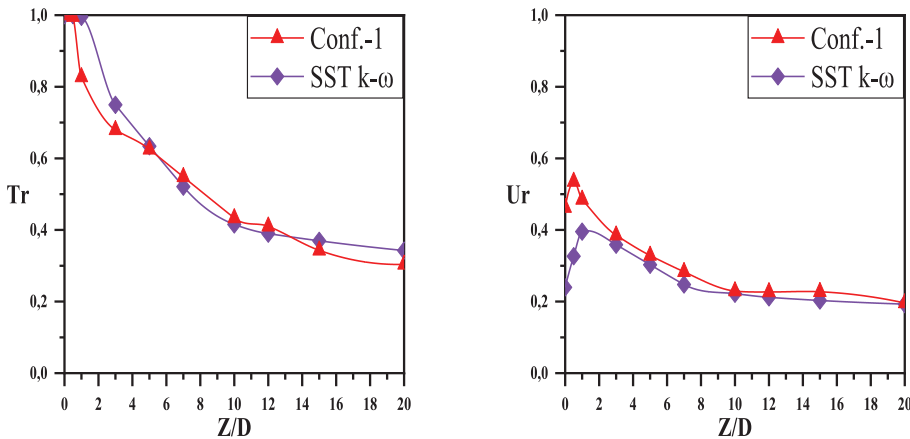


Figure 13. Comparison of the experimental and numerical axial velocity profiles configuration 1.

radial velocity and temperature at the different axial stations, provided by the model SST k- $\omega$ . The observed SST k- $\omega$  perfectly predicts the velocity distribution and temperature profiles coincide well with experimental measurements.

The average error between the model results and the experimental, for velocity profiles, and for temperature in the table following.

**Velocity and Temperature (Axial Distribution) for Configuration 2**

In Figure 16, the numerical results are derived using the SST k- $\omega$  turbulence model. Good agreement was obtained

between the expected temperature and velocity profiles with the turbulence model SST k- $\omega$  and experimental results. In the axial direction, the root means square error between the results obtained using the turbulence model SST k- $\omega$  and the experimental results for velocity was 0.05461476, and the temperature was 0.03440311.

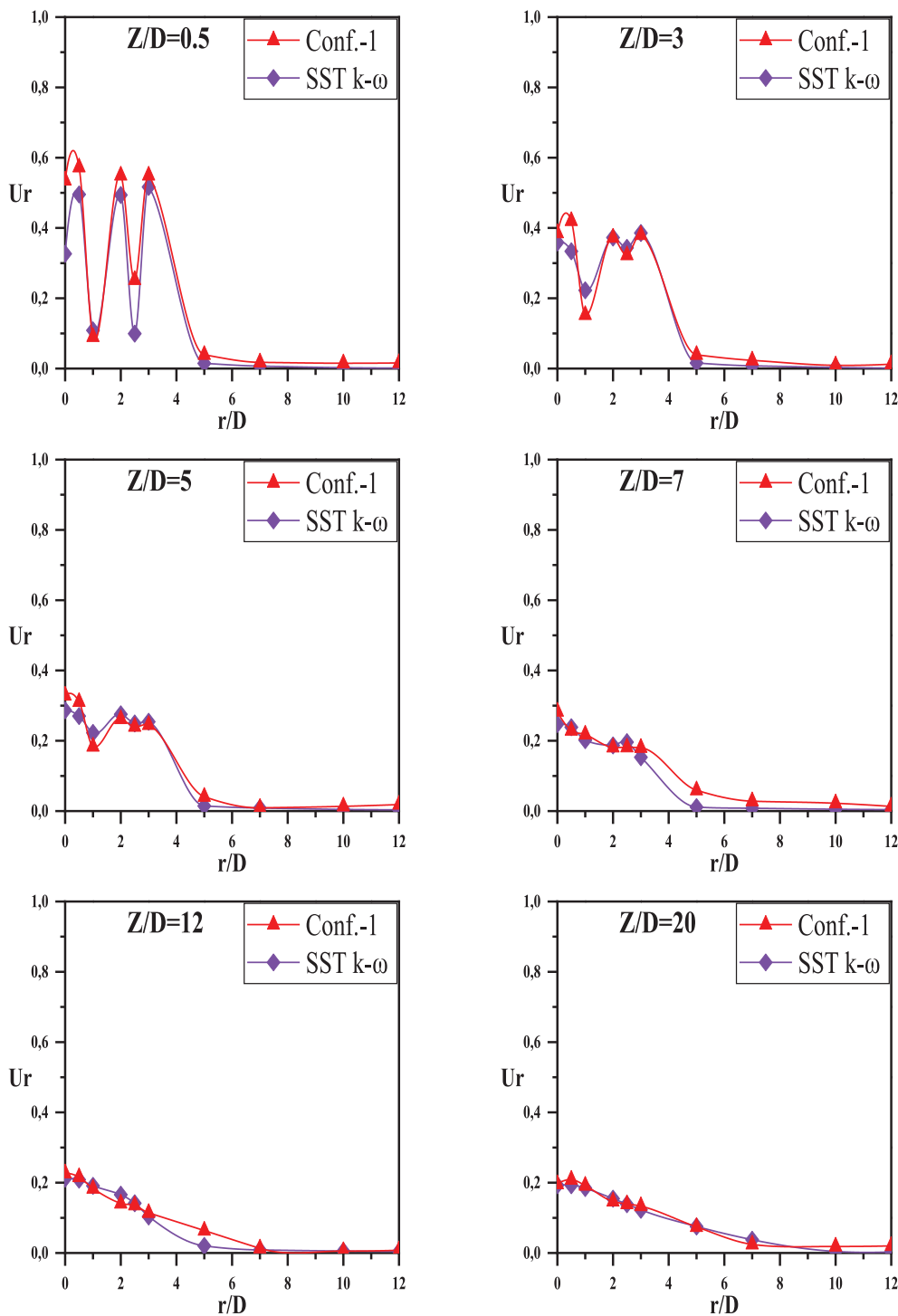
For configuration 2, Figure 17 shows the radial velocity features and Figure 18 shows the radial temperature features. Numerically, the turbulence model SST k- $\omega$  was used and its results were compared with the experimental results, where the axial dimension from 0.5-20 was studied. The error rate is shown in Table 4.

Table 3. Root Mean Square Error between model SST k- $\omega$  and experiment results for configuration 1

| RMS Error SST k- $\omega$ |          | RMS Error SST k- $\omega$ |           |          |            |
|---------------------------|----------|---------------------------|-----------|----------|------------|
| Radial velocity           |          | Radial Temperature        |           |          |            |
| Figure 14                 | Z/D =0.5 | 0.08849552                | Figure 15 | Z/D =0.5 | 0.14937118 |
|                           | Z/D =3   | 0.03813832                |           | Z/D =3   | 0.0948848  |
|                           | Z/D =5   | 0.02506777                |           | Z/D =5   | 0.05849392 |
|                           | Z/D =7   | 0.2234185                 |           | Z/D =7   | 0.06236248 |
|                           | Z/D =12  | 0.01743728                |           | Z/D =12  | 0.04384145 |
|                           | Z/D =20  | 0.01068651                |           | Z/D =20  | 0.02595294 |

Table 4. Root Mean Square Error between model SST k- $\omega$  and experiment results for configuration 2

| RMS Error SST k- $\omega$ |          | RMS Error SST k- $\omega$ |           |          |            |
|---------------------------|----------|---------------------------|-----------|----------|------------|
| Radial velocity           |          | Radial Temperature        |           |          |            |
| Figure 17                 | Z/D =0.5 | 0.16956651                | Figure 18 | Z/D =0.5 | 0.15894701 |
|                           | Z/D =3   | 0.03619725                |           | Z/D =3   | 0.05071068 |
|                           | Z/D =5   | 0.03280496                |           | Z/D =5   | 0.04303284 |
|                           | Z/D =7   | 0.03252151                |           | Z/D =7   | 0.02483038 |
|                           | Z/D =12  | 0.02915016                |           | Z/D =12  | 0.02915773 |
|                           | Z/D =20  | 0.01620156                |           | Z/D =20  | 0.02517794 |



**Figure 14.** Comparison of the experimental and numerical radial velocity profiles.

The average error between the model results and the experimental, for velocity profiles, and for temperature in the table following.

In Figure 19, the numerical and experimental results for lower temperature and velocity in various axial positions are compared. The numerical results are derived using the

SST k- $\omega$  turbulence model. Good agreement was obtained between the expected temperature and velocity profiles with the turbulence model SST k- $\omega$  and experimental results. For temperature profiles in the range  $Z/D = 1$  to  $Z/D = 5$ , the turbulence model departed somewhat from the correct prediction. In the axial direction, the root means square error

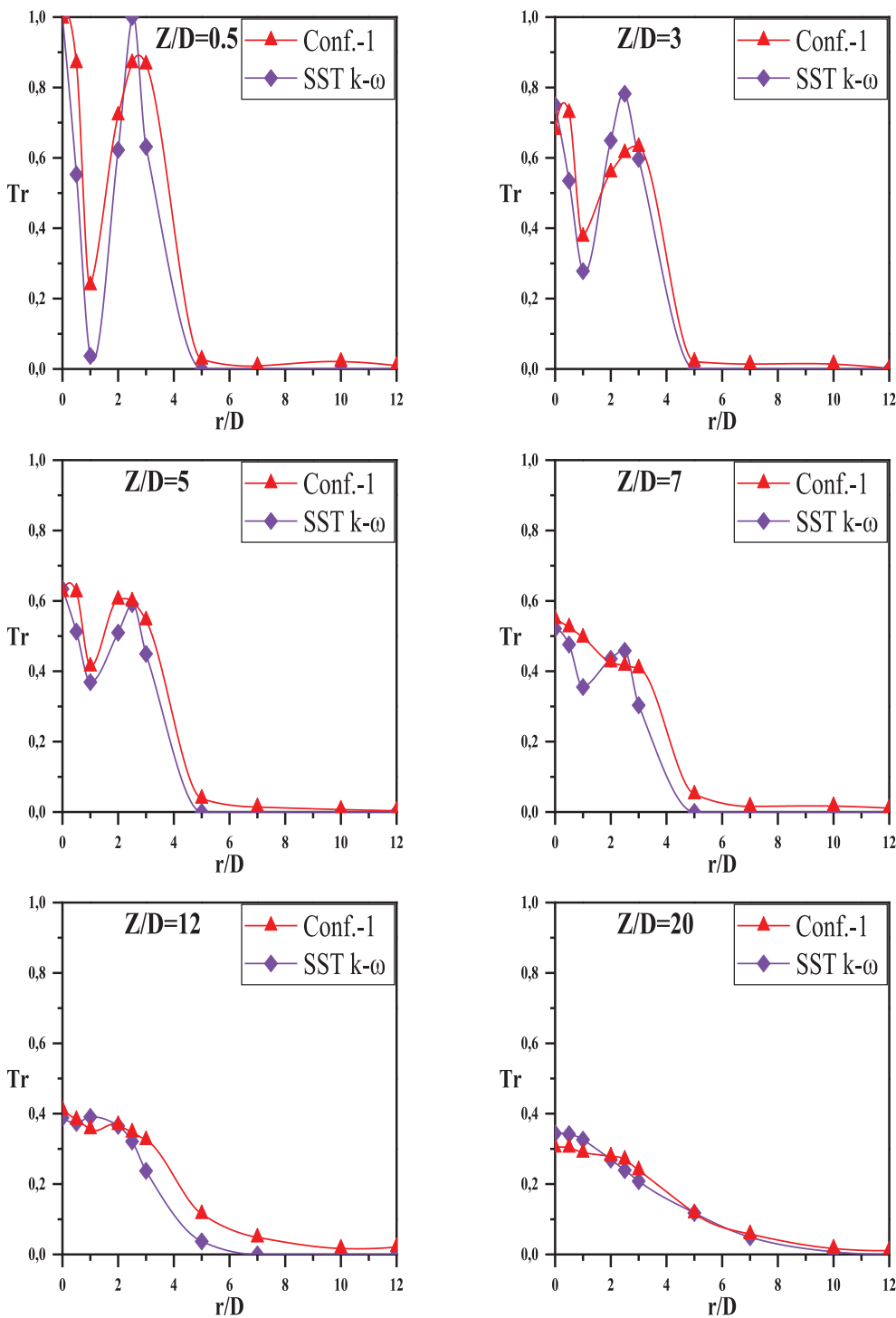


**Figure 15.** Comparison of the experimental and numerical radial temperature profiles.

(RMSE) between the results obtained using the turbulence model SST k- $\omega$  and the experimental results for velocity was 0.01897281, and the temperature was 0.06107762.

The reduced Velocity and Temperature radial profiles are shown in Figure 20 (velocity), and Figure 21

(Temperature) and compared with the experimental values at  $Z/D = 0.5, 3, 5, 7, 12$  and 20 in the major plane.

For  $Z/D=0.5$  to 20, the radial temperatures and velocity predicted with the SST k- $\omega$  Turbulence model were well validated with the experimental results, The root means

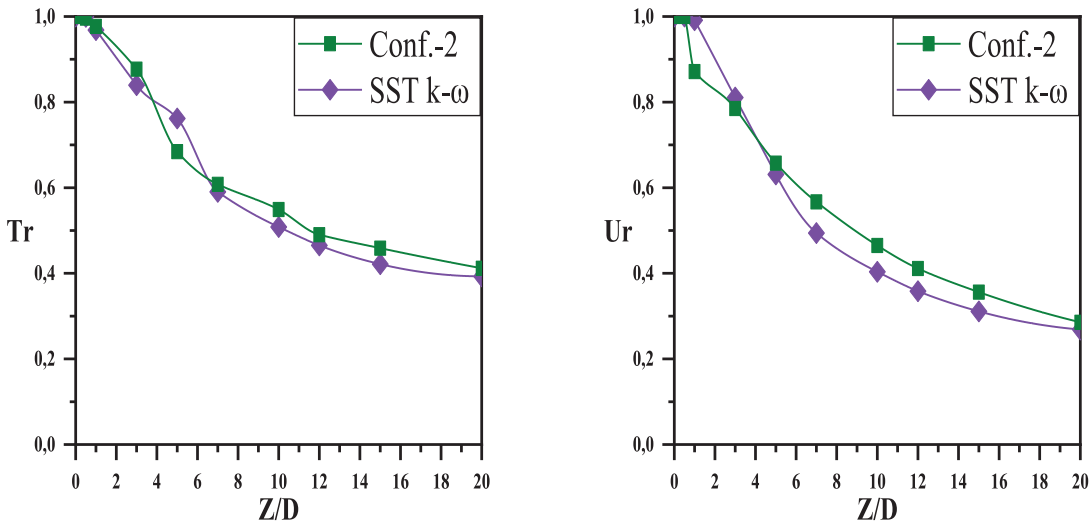


Figure 16. Comparison of the experimental and numerical axial velocity profiles configuration 2.

Table 5. Root Mean Square Error between model SST k- $\omega$  and experiment results for configuration 3

| RMS Error SST k- $\omega$ |          | RMS Error SST k- $\omega$ |          |            |
|---------------------------|----------|---------------------------|----------|------------|
| Radial velocity           |          | Radial Temperature        |          |            |
| Figure 20                 | Z/D =0.5 | 0.08044512                | Z/D =0.5 | 0.14961496 |
|                           | Z/D =3   | 0.03361872                | Z/D =3   | 0.06502914 |
|                           | Z/D =5   | 0.0502611                 | Z/D =5   | 0.05156491 |
|                           | Z/D =7   | 0.055257                  | Z/D =7   | 0.03781148 |
|                           | Z/D =12  | 0.02530421                | Z/D =12  | 0.04043994 |
|                           | Z/D =20  | 0.02301708                | Z/D =20  | 0.02395498 |

square error between the SST k- $\omega$  model results and the experimental results shows in Table 5.

**Temperature Contours**

Figure 22 shows the average temperature contours From the SST k- $\omega$  model on different axes stations (Z/D = 0.5, 3, 5, 7, 12, 20). The third region seems to show in the result of the experiments. The first region smaller than position Z/D=3 extends over the beam diameter The exit is where the peripheral jets start to mix with the rays Ambient air is drawn into the central jet but there is no interaction between the jets themselves. In the second region between Z/D stations = 3 and Z/D = 7, the jets interact and merge in the process Ensuring that the resulting beam spreads.

Third region greater than position Z/D = 7, where the temperature profiles should be evenly combined into a Circular beam profile towards the station Z/D = 20 where the resulting beam temperature is close to ambient temperature.

**Velocity Contours**

Figure 23 shows the Velocity contours for the three configurations at six different downstream stations (Z/D = 0.5, 3, 5, 7, 12 and 20). the homogenization of aircraft from Station Z/D = 3 begins in the three configurations with little preference for the third configuration. This is due to the central vortex jet. The homogeneity is apparent from the beginning of Z/D = 5, It should be noted that the form of the jet plays a significant role in the homogenization process, especially if it is in the position of the center.

**Turbulence Intensity Contours**

Figure 24 shows the turbulence intensity contours for the three configurations at six different downstream stations (Z/D = 0.5, 3, 5, 7,12 and 20). Z / D = 3. It can be seen that from this station the third configuration was given the lowest value for the turbulence intensity in the potential core and this is due to its conversion to intensity in the radial direction, this indicates the intensity and speed of mixing the central jet streams with the ambient jets for the Configuration 3. For Configurations 1 and 2, the central

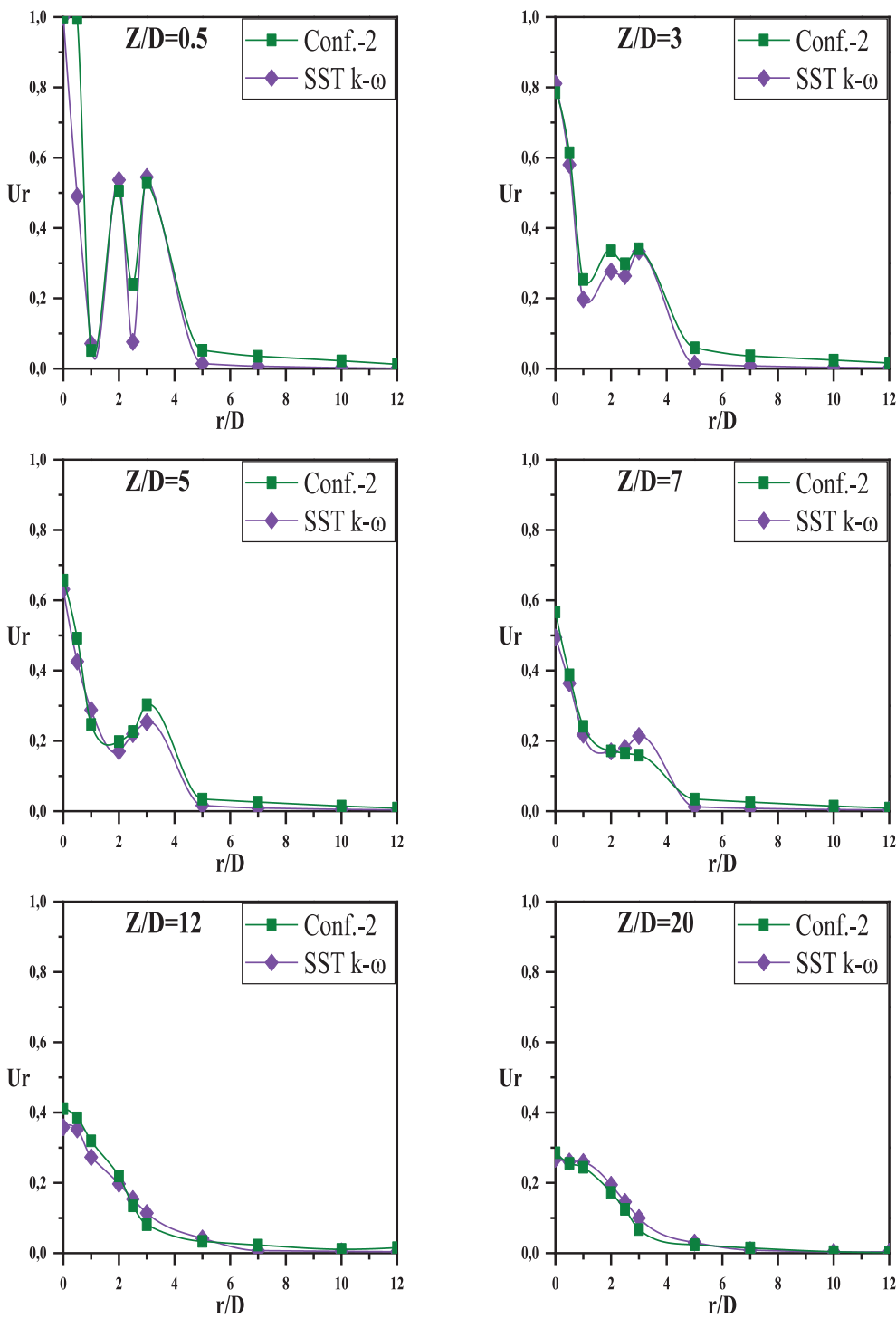


Figure 17. Comparison of the experimental and numerical radial velocity profiles.

jet remains more influential in the axial direction, and this is shown by the clear turbulence intensity contours on the center of these two Configurations.

**Turbulent Kinetic Energy (K) Contours**

In the range  $Z/D=0.5 - 20$ , Figure 25 shows turbulent kinetic energy contours vs. axial distance. It has been

observed that the contours of turbulent kinetic energy decreased with increasing distance in the axial direction. In the first stations, the features of the configuration are clear and then begin to merge with each other until they become behaving as a single jet, and it can be seen that the SST k- $\omega$  turbulence model agrees well with the experimental results.

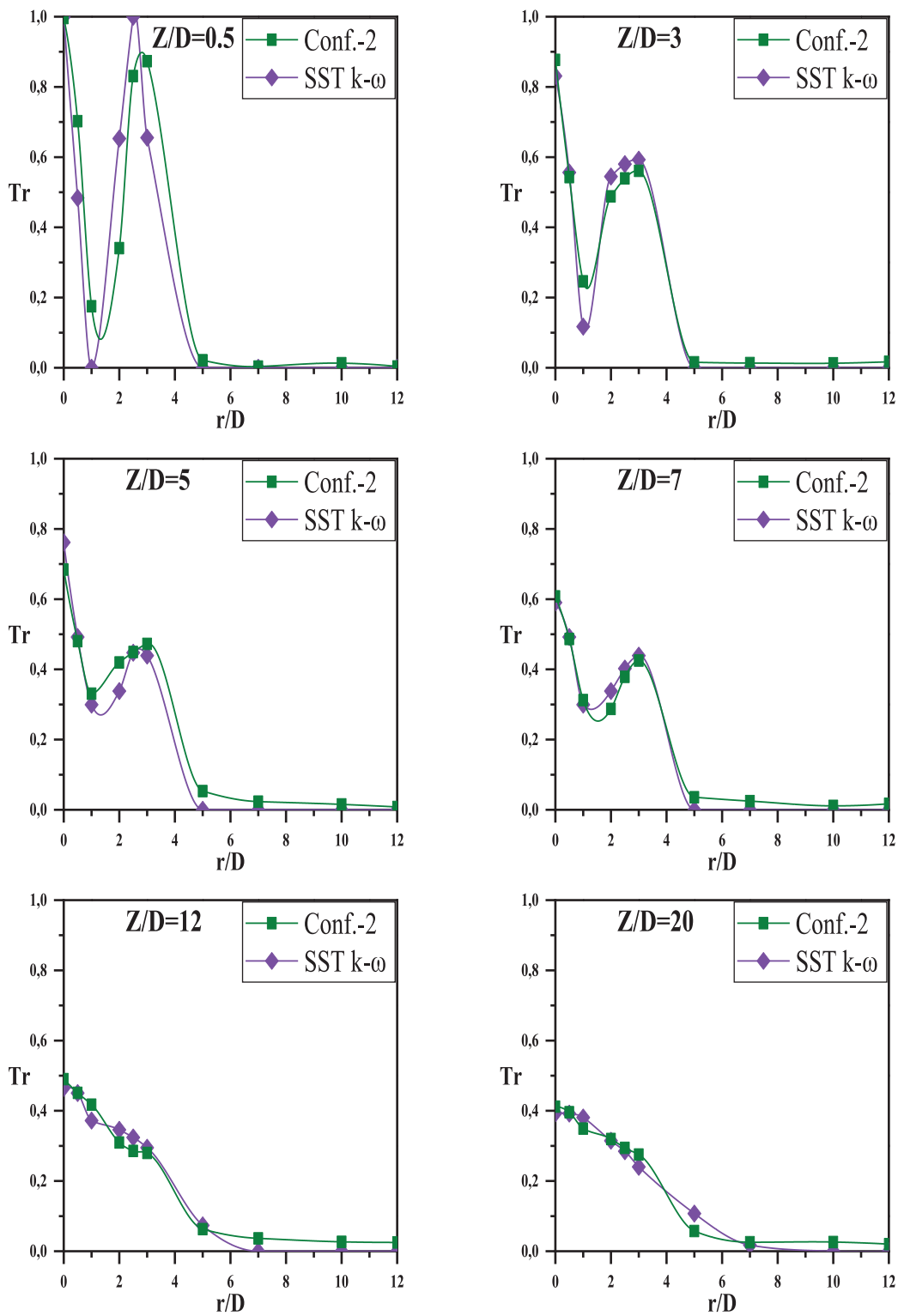


Figure 18. Comparison of the experimental and numerical radial temperature profiles.

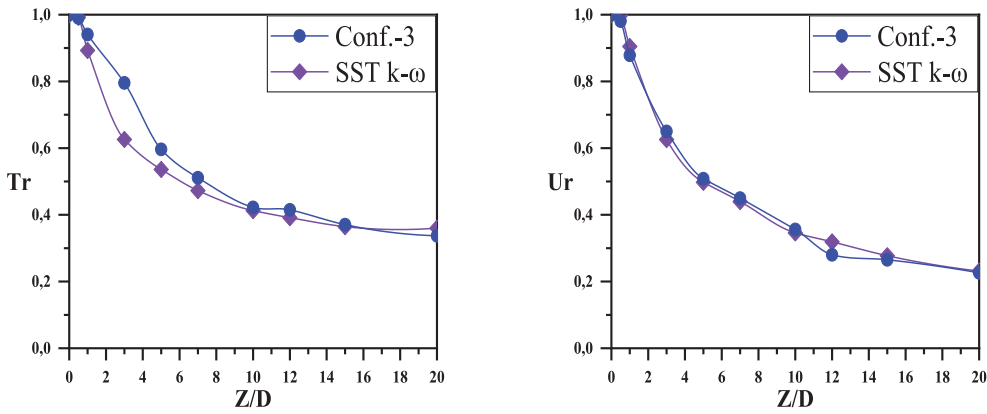


Figure 19. Axial Temperature and velocity profiles for configuration 3.

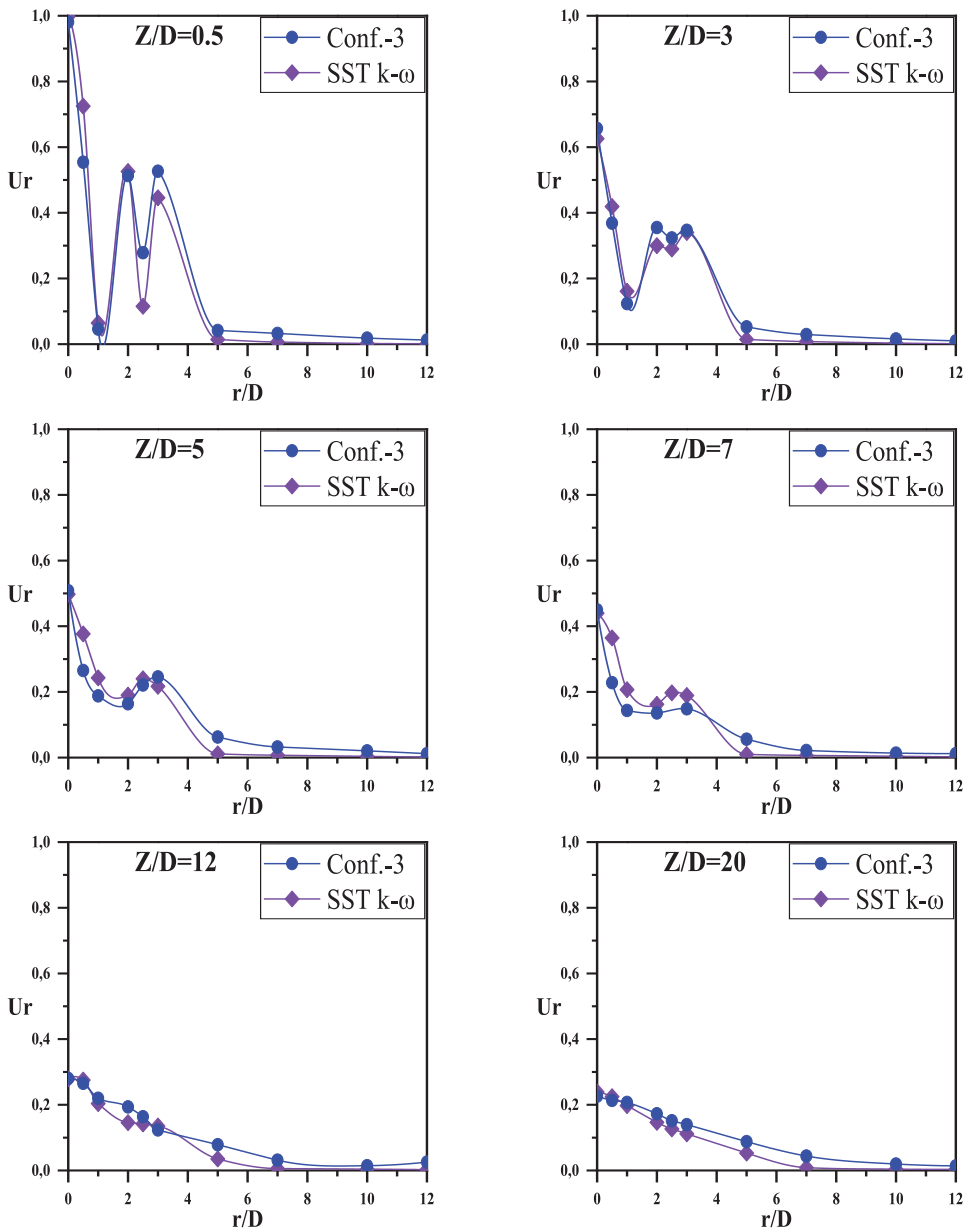


Figure 20. Comparison of the experimental and numerical radial velocity profiles.

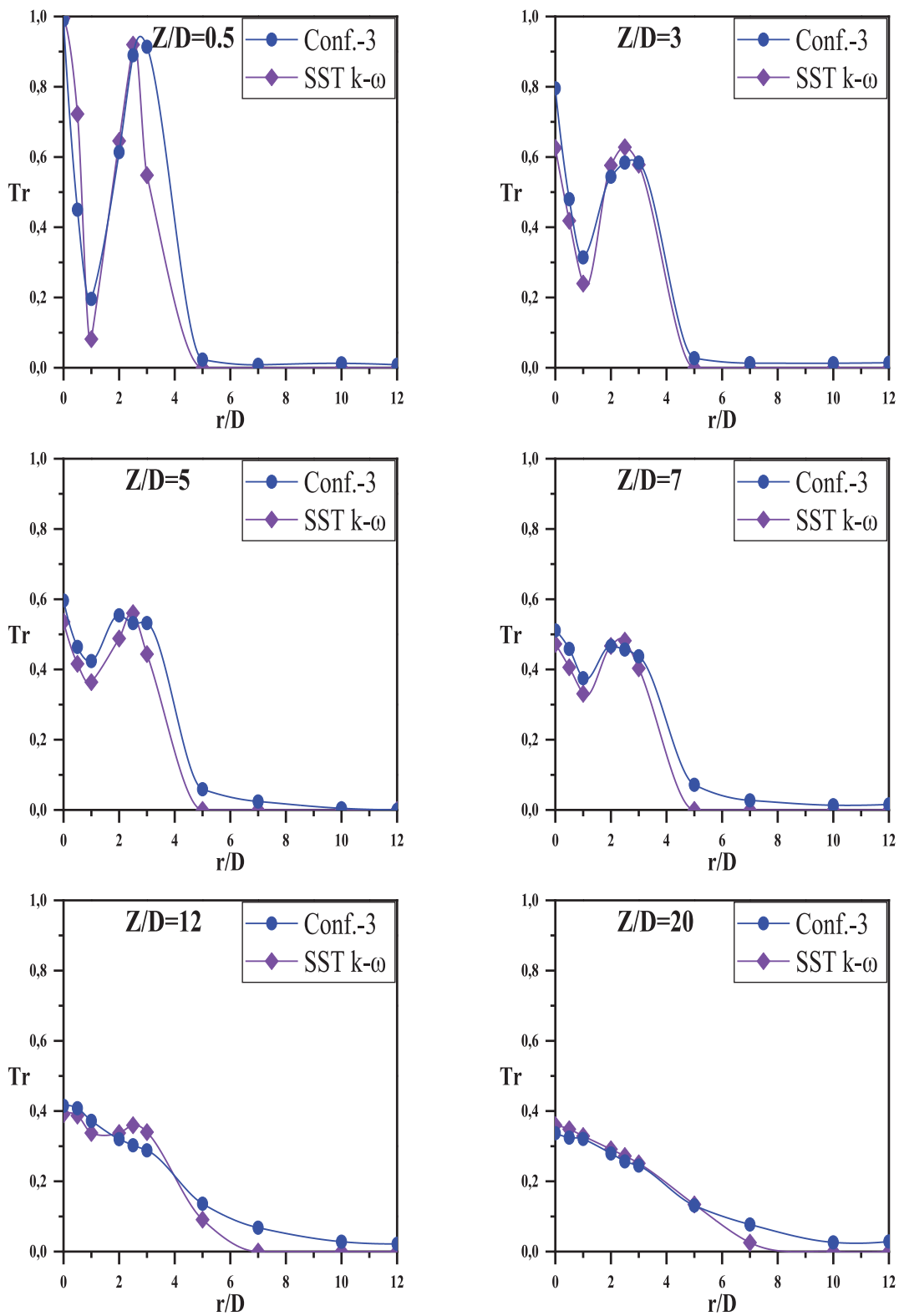


Figure 21. Comparison of the experimental and numerical radial temperature profiles.

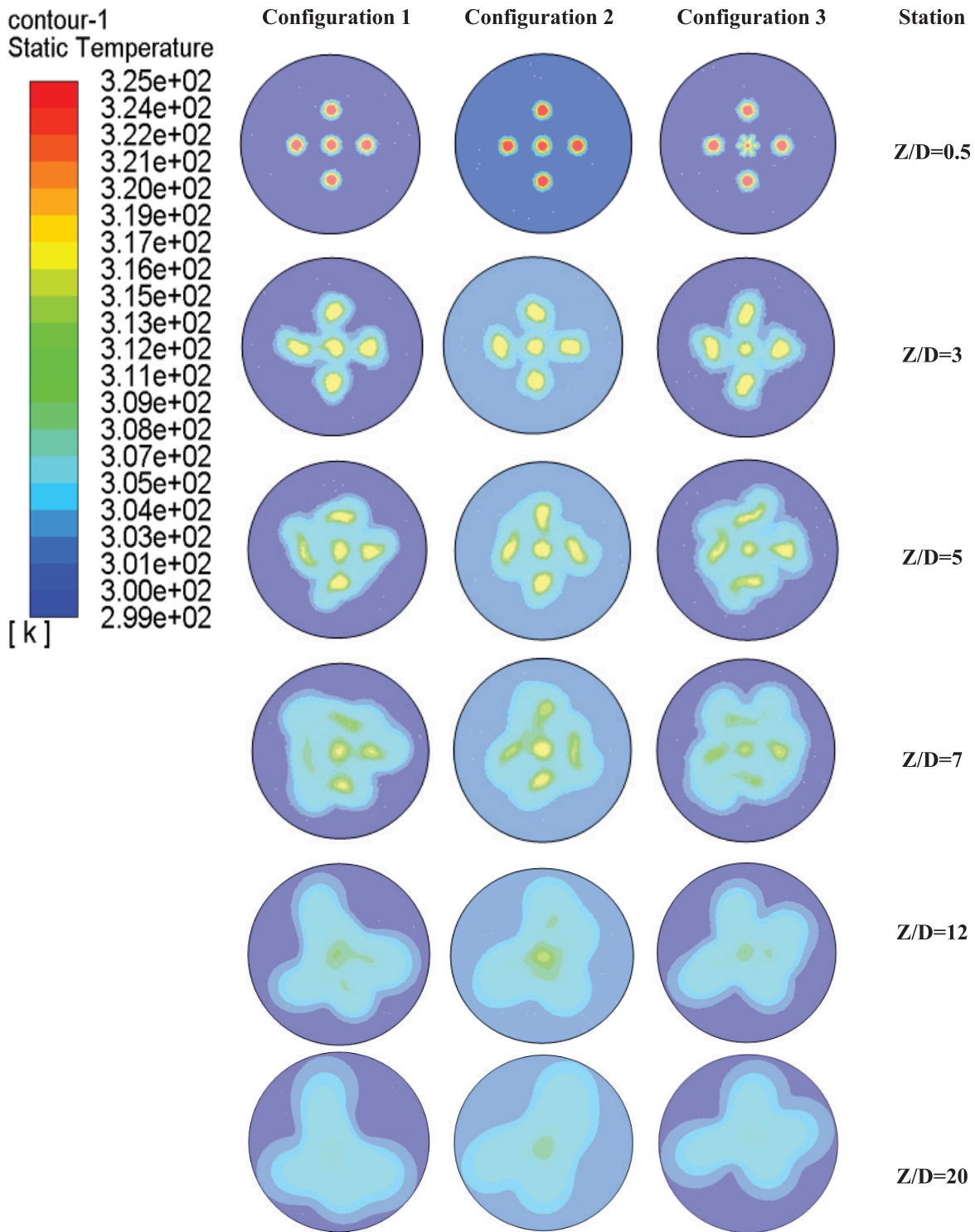


Figure 22. Simulated average temperature contours with the SST k- $\omega$  model.

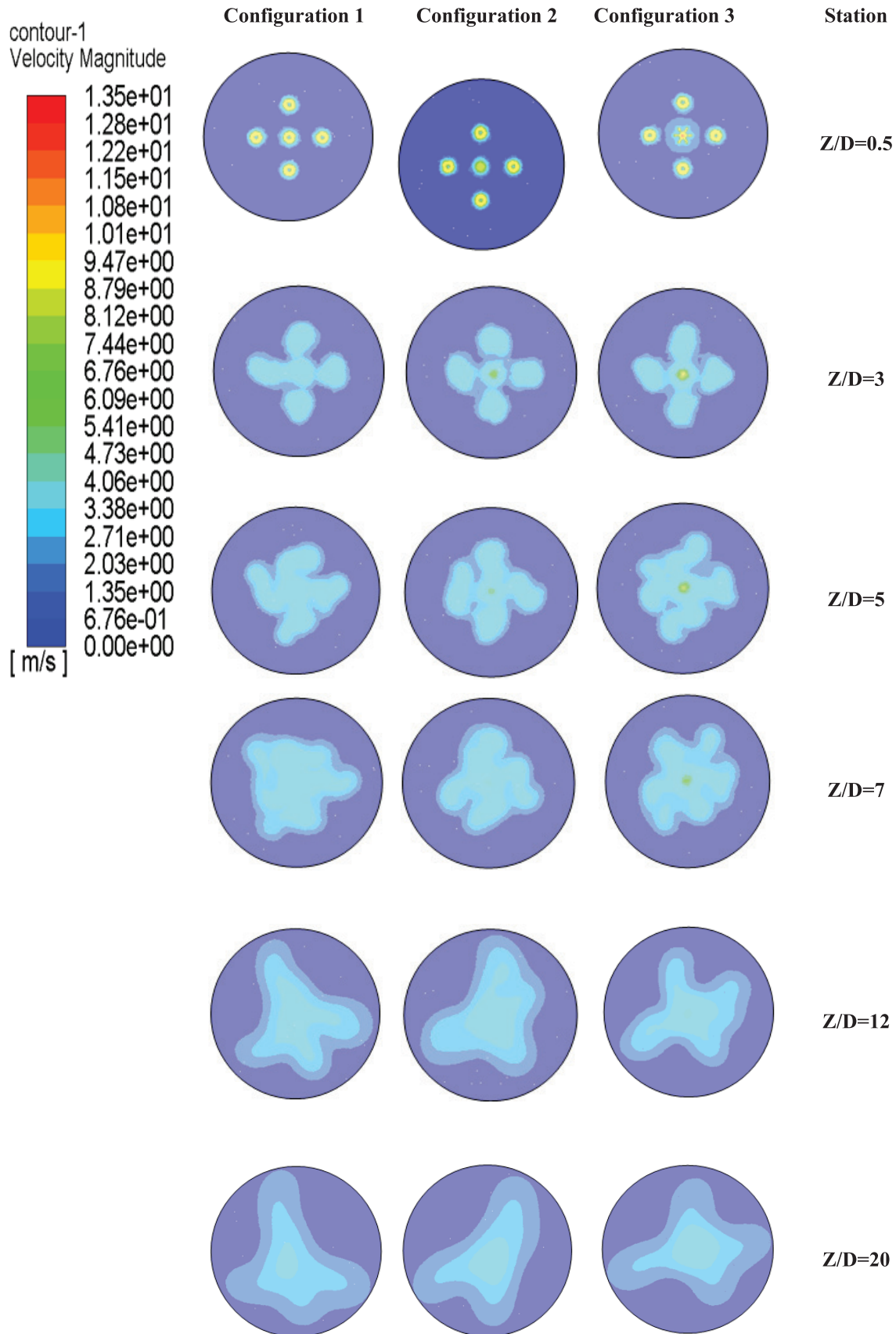


Figure 23. Simulated average velocity contours with the SST k- $\omega$  model.

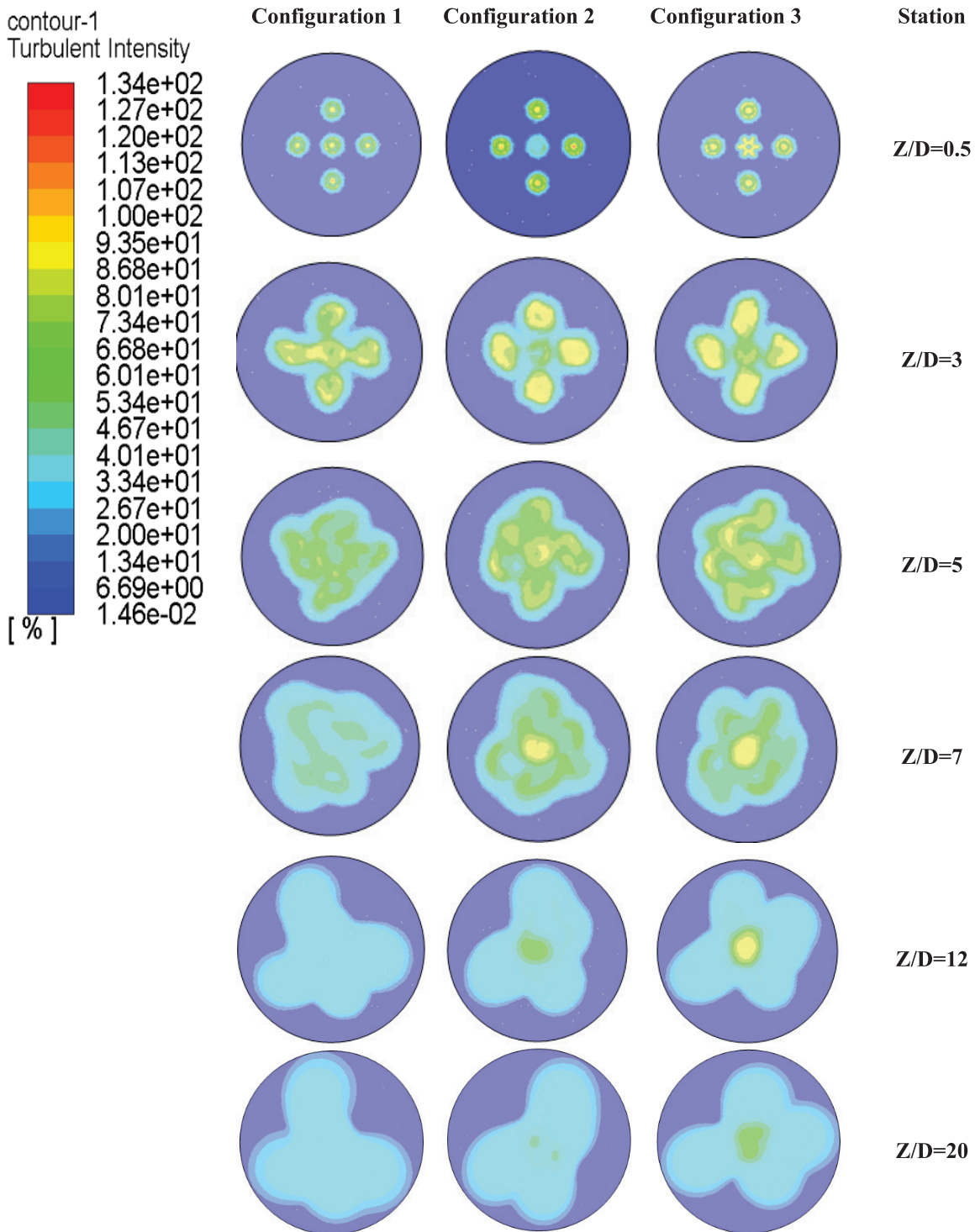


Figure 24. Simulated average turbulence intensity contours with the SST k- $\omega$  model.

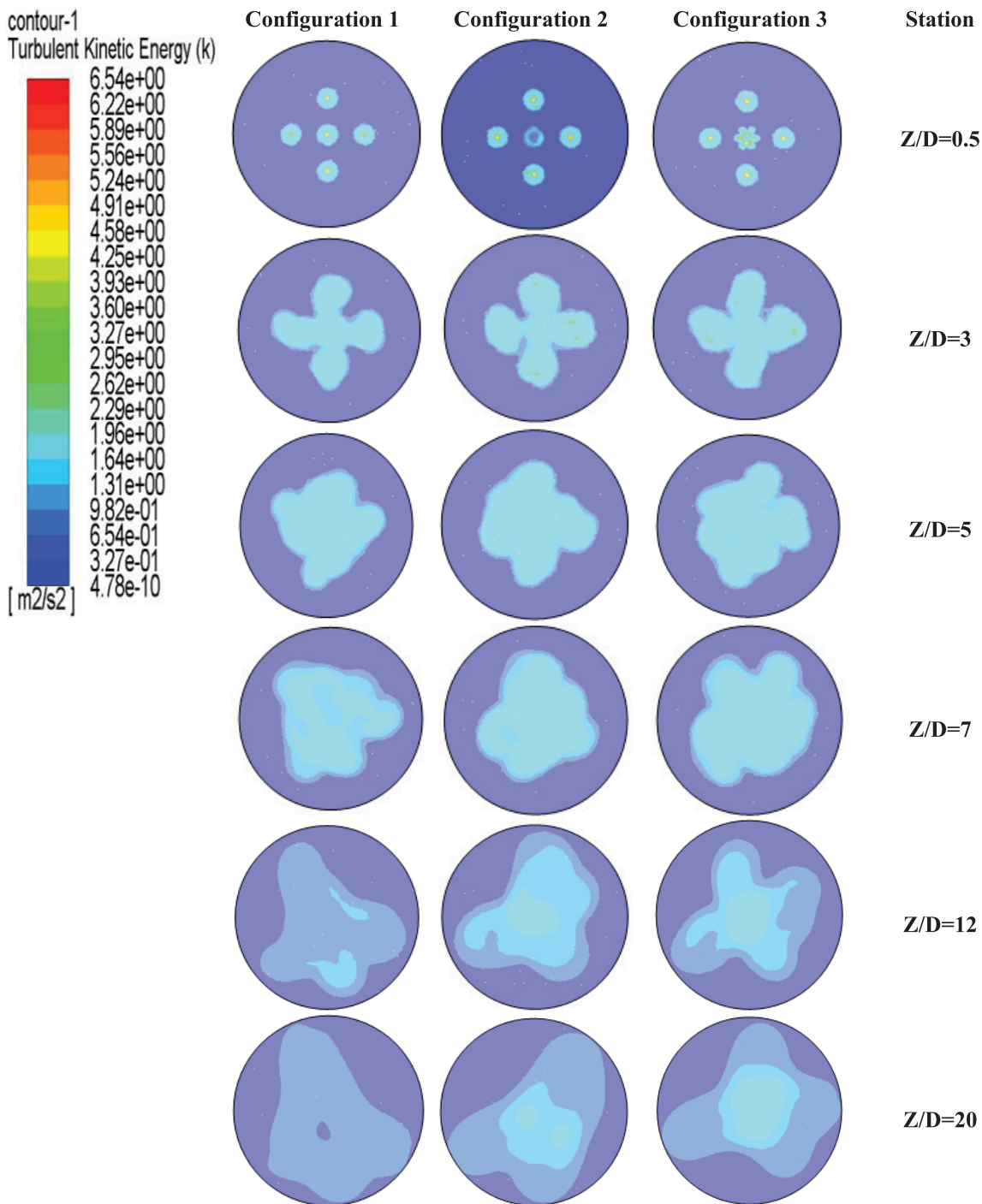


Figure 25. Simulated average turbulent kinetic energy (k) contours with the SST k- $\omega$  model.

### CONCLUSION

In this study, explored different configurations of blowing multiple jets for using in ventilation and heating and air conditioning systems used in the premises. The originality of this study is to meet the requirements of occupants in terms of thermal comfort and air quality by proposing an optimal solution for the thermal homogenization

improvement field in the rooms by changing of the diffusers geometry and their arrangement in the ventilation and air-conditioning devices in blowing systems. This study, highlighted more improvement of the thermal and dynamic homogenization using three cases of configurations that were considered, central swirling jet surrounded by four equidistant peripheral swirling jets, central circular jet surrounded by four peripheral swirling jets and central

lobed jet surrounded by four peripheral swirling jets. The study was carried out experimentally and numerically, and the following conclusions were given:

- Analysis of the axial and radial temperature profiles highlighted the importance and the role of the central jet type in the mixing performance of the airflow.
- Configuration 3 was observed to result in a wider jet flow and to intensify mixing compared to configuration 2 and configuration 1.
- That the lobed jet ensures a better spreading of the radial temperatures and radial velocity compared to the swirling jet and circular jet.
- The circular jet provides better stability in axial velocity and axial temperature than swirling jet and lobed jet.
- The SST  $k-\omega$  turbulence model is capable to predict properly the jets' interaction, the dynamic and thermal expansion and the entrapment of ambient air for volume flow from swirling, circular and lobed diffusers.
- Our results show that the geometry of the central diffuser is essential. This allows the axial velocity to decrease faster than configurations 1 and 2. This increases lateral diffusion, resulting in better homogenization.

## AUTHORSHIP CONTRIBUTIONS

Authors equally contributed to this work.

## DATA AVAILABILITY STATEMENT

The authors confirm that the data that supports the findings of this study are available within the article. Raw data that support the finding of this study are available from the corresponding author, upon reasonable request.

## CONFLICT OF INTEREST

The author declared no potential conflicts of interest with respect to the research, authorship, and/or publication of this article.

## ETHICS

There are no ethical issues with the publication of this manuscript.

## REFERENCES

- [1] Nawale PR, Mule AA, Powar SB, Kothmire PP. Enhancement technique of heat transfer using inserted twisted tape. *J Therm Engineer* 2021;7:1614–1627. [\[CrossRef\]](#)
- [2] Badiger S, Katti VV, Anil TR. Experimental investigation of heat transfer characteristics of an inverse diffusion flame in a coaxial tube burner for with and without swirl. *J Therm Engineer* 2022;8:67–77. [\[CrossRef\]](#)
- [3] Senveli A, Dizman T, Celen A. Cfd Analysis of smoke and temperature control system of an indoor parking lot with jet fans. *J Therm Engineer* 2015;1:116–130. [\[CrossRef\]](#)
- [4] Cherrared D. Numerical simulation of film cooling a turbine blade through a row of holes. *J Therm Engineer* 2017;3:1110–1120. [\[CrossRef\]](#)
- [5] Dash SC, Singh N. Study of, axisymmetric nature in 3 d swirling flow in a cylindrical annulus with a top rotating lid under the influence of axial temperature gradient or axial magnetic field. *J Therm Engineer* 2017;3:1588–1606. [\[CrossRef\]](#)
- [6] Kravtsov ZD, Sharaborin DK, Dulin VM. Swirl effect on flow structure and mixing in a turbulent jet. *J Physics: Conference Series* 2018;012001. [\[CrossRef\]](#)
- [7] Meslem A, Nastase I, Abed-Meraim K. Experimental investigation of a lobed jet flow mixing performance. *J Eng Phys Thermophys* 2008;81:106–111. [\[CrossRef\]](#)
- [8] Medaouar W, Loukarfi L, Braikia M, Khelil A, Naji H. Experimental and numerical study of a turbulent multiple jets issued from lobed diffusers. *J Appl Fluid Mech* 2019;12:729–742.
- [9] Felli M, Falchi M, Pereira F. Distance effect on the behavior of an impinging swirling jet by PIV and flow visualization. *Exp Fluids* 2009; 48:197–209. [\[CrossRef\]](#)
- [10] Lee SG. Experimental investigation of mixing enhanced swirl flows. *J Mech Sci Technol* 2008;22:2509–2515. [\[CrossRef\]](#)
- [11] Meslem A, Nastase I, Allard F. Passive mixing control for innovative air diffusion terminal devices for buildings. *Building Environ* 2010;45:2679–2688. [\[CrossRef\]](#)
- [12] Meslem A, Greffet R, Nastase I, Ammar A. Experimental investigation of jets from rectangular six-lobed and round orifices at very low Reynolds number. *Meccanica* 2014;49:2419–2437. [\[CrossRef\]](#)
- [13] Bennia A, Loukarfi L, Braikia M, Khelil A, Naji H. Etude expérimentale d'un jet turbulent à diffuseur muni de lobes : Application au confort dans les locaux à usage d'habitation. *Nature & Technologie. A Sciences fondamentales and Engineering* 2015;13:54–58.
- [14] Nuntadusit C, Waehayee M, Bunyajitradulya A, Eiam Saard S. Heat transfer enhancement by multiple swirling impinging jets with twisted-tape swirl generators. *Int Comm Heat Mass Transf* 2012;39:102–107. [\[CrossRef\]](#)
- [15] Maurel S, Rey C, Sollicc C. Comparison modeling experience in the case of a turbulent air jet impinging a plate planes. *School of Mines Nantes. XVth French Congress of Mechanics Nancy, 3 to 7 2001.*
- [16] Alekseenko SV, Bilsky AV, Dulin VM, Markovich DM. Experimental study of an impinging jet with different swirl rates. *Int J Heat Fluid Flow* 2007;28:1340–1359. [\[CrossRef\]](#)

- [17] Xu L, Zhao X, Xi L, Ma Y, Gao J, Xi L, et al. Large-eddy simulation study of flow and heat transfer in swirling and non-swirling impinging jets on a semi-cylinder concave target. *Appl Sci* 2021;11:7167. [\[CrossRef\]](#)
- [18] Kannan BT. Computation of an axisymmetric jet using OpenFOAM. *Procedia Engineer* 2015;127:1292–1299. [\[CrossRef\]](#)
- [19] Nastase I, Meslem A, Vlad I, Colda I. Lobed grilles for high mixing ventilation-An experimental analysis in a full scale model room. *Building Environ* 2011;46:547–555. [\[CrossRef\]](#)
- [20] Braikia M, Loukarfi L, Khelil A, Naji H. Improvement of thermal homogenization using multiple swirling jets. *Therm Sci* 2012;16:239–250. [\[CrossRef\]](#)
- [21] Khelil A, Naji H, Loukarfi L, Meliani MH, Braikia M. Numerical simulation of the interactions among multiple turbulent swirling jets mounted in unbalanced positions. *Appl Math Model* 2016;40:3749–3763. [\[CrossRef\]](#)
- [22] Bragança P, Sodjavi K, Meslem A. Passive control strategy for mixing ventilation in heating and cooling modes using lobed inserts. *Energy Procedia* 2017;112:232–239. [\[CrossRef\]](#)
- [23] Depuru Mohan NK, Prakash KR, Panchapakesan NR. Mixing augmentation by multiple lobed jets. *Am J Fluid Dynamics* 2015;5:55–64.
- [24] Bennia A, Loukarfi L, Khelil A, Mohamadi S, Braikia M, Naji N. Contribution to the experimental and numerical dynamic study of a turbulent jet issued from lobed diffuser. *J Appl Fluid Mech* 2016;9:2957–2967.
- [25] Boussoufi M, Sabeur-Bendehina A, Ouadha A, Morsli S, El Ganaoui M. Numerical analysis of single and multiple jets. *European Physical J Appl Physics* 2017;78:34814. [\[CrossRef\]](#)
- [26] Bagre N, Parekh AD, Pate VK. A CFD investigation of flow separation in an elliptical and circular ranque-hilsch vortex tube. *J Therm Engineer* 2023;9. [\[CrossRef\]](#)
- [27] Ravi D, Rajagopal TKR. Numerical investigation on the effect of slit thickness and outlet angle of the bladeless fan for flow optimization using CFD techniques. *J Therm Engineer* 2023;9. [\[CrossRef\]](#)
- [28] Menter F. Zonal two equations kw turbulence models for aerodynamic flows. 23rd Fluid Dynamics, Plasmadynamics, and Lasers Conference; 1993. p. 2906. [\[CrossRef\]](#)
- [29] Menter FR. Two-equation eddy-viscosity turbulence models for engineering applications. *AIAA J* 1994;32:1598–1605. [\[CrossRef\]](#)
- [30] Menter FR. Review of the shear-stress transport turbulence model experience from an industrial perspective. *Int J Comput Fluid Dynamics* 2009;23:305–316. [\[CrossRef\]](#)
- [31] Hassan M, Mebarek-Oudina F, Faisal A, Ghafar A, Ismail AI. Thermal energy and mass transport of shear thinning fluid under effects of low to high shear rate viscosity. *Int J Thermofluids* 2022;15:100176. [\[CrossRef\]](#)
- [32] Laouira H, Mebarek-Oudina F, Hussein AK, Kolsi L, Merah A, Younis O. Heat transfer inside a horizontal channel with an open trapezoidal enclosure subjected to a heat source of different lengths. *Heat Transf* 2020;49:406–423. [\[CrossRef\]](#)
- [33] Mebarek-Oudina F, Laouira H, Aissa A, Hussein AK, El Ganaoui M. Convection heat transfer analysis in a channel with an open trapezoidal cavity: Heat source locations effect. *MATEC Web of Conferences ICOME'19* 2020;330:01006. [\[CrossRef\]](#)
- [34] Gourari S, Mebarek-Oudina F, Makinde OD, Rabhi M. Numerical investigation of gas-liquid two-phase flows in a cylindrical channel. *Engineer Fluid Flows Heat Transf Anal* 2021;409:39–48. [\[CrossRef\]](#)
- [35] Mebarek-Oudina F, Laouira H, Hussein AK, Omri M, Abderrahmane A, Kolsi L, et al. Mixed convection inside a duct with an open trapezoidal cavity equipped with two discrete heat sources and moving walls. *Mathematics* 2022;10:929. [\[CrossRef\]](#)